applied sciences

MDPI

Article

Influence of Quantum Effects on Dielectric Relaxation in Functional Electrical and Electric Energy Elements Based on Proton Semiconductors and Dielectrics

Valeriy Kalytka [1,*], Zein Baimukhanov [2,*], Yelena Neshina [1], Ali Mekhtiyev [3,*], Pavel Dunayev [3], Olga Galtseva [4] and Yelena Senina [1]

[1] Faculty of Energy, Automation and Telecommunications, Abylkas Saginov Karaganda Technical University, Karaganda 100027, Kazakhstan; 1_neg@mail.ru (Y.N.); komir-kuat_senina@mail.ru (Y.S.)
[2] Faculty of Technical Physics, L.N. Gumilyov Eurasian National University, Astana 010008, Kazakhstan
[3] Energy Department, S. Seifullin Kazakh Agro Technical Research University, Astana 010011, Kazakhstan; dunayev.kz@mail.ru
[4] School of Non-Destructive Testing, National Research Tomsk Polytechnic University, Tomsk 634050, Russia; piano@tpu.ru
* Correspondence: manuscript.kz@bk.ru or valerii.kalytka@gmail.com (V.K.); zbaimukhanov@list.ru (Z.B.); ali.mekhtiyev.99@bk.ru (A.M.); Tel.: +7-7212-56-44-22 (V.K.)

Abstract: Using the quasi-classical kinetic theory of dielectric relaxation, in addition to existing methods, fundamental mathematical expressions are built, which make it possible to more strictly consider the effects of the main charge carriers' (protons') tunneling on the numerical values of the molecular parameters (activation energy, equilibrium concentration) of protons in HBC. The formulas for calculating the statistically averaged non-stationary quantum transparency of a parabolic potential barrier for protons have been modernized by more stringent consideration of the effects of corrections caused by an external electric field. For the model of a double-symmetric potential well, a generalized nonlinear solution of the quasi-classical kinetic equation of dielectric relaxation in HBC was built. The phenomenological Bucci-Rive formula for thermally stimulated depolarization current density (TSDC) was first investigated, taking into account quantum transparency, for the case of a parabolic potential barrier. The choice of the parabolic shape of the potential barrier allowed, at a theoretical level, for the mathematical model of relaxation polarization to be brought closer to the conditions of the real spatial structure of the crystal potential field, in comparison with the rectangular potential barrier model. It has been found that quantum effects due to proton tunnel transitions significantly affect the mechanism of thermally stimulated depolarization currents in HBC, over a wide temperature range (50–550 K) and external field parameters (0.1–1 MV/m). Generalized solutions of the nonlinear kinetic equation, recorded considering the effects of field parameters on proton tunnel transitions, made it possible to significantly approximate the theoretical values of activation energies, equilibrium concentrations of protons and amplitudes of the theoretical maxima of the current density of thermally stimulated depolarization, according to their experimental values in the field of low-temperature (50–100 K) and high-temperature (350–550 K) maxima of TSDC density in HBC. For the first time, precision measurements of TSDC temperature spectra were carried out for chalcanthite crystals. The effects of alloying impurities concentrations and crystal calcination temperatures on the parameters of experimental maxima in the TSDC spectrum of chalcanthite were established. A physical mechanism of the quantum tunnel motion of protons in HBC with a complex crystal structure (crystalline hydrates, layered silicates, ferroelectric HBC (KDP, DKDP)) is described. The patterns found in this article indicate a fairly high degree of applied scientific significance for the obtained theoretical results, allowing for the further development of electrophysics and optoelectronics of heterogeneous structures (MIS, MSM) based on proton semiconductors and dielectrics (PSD) and their composites.

Citation: Kalytka, V.; Baimukhanov, Z.; Neshina, Y.; Mekhtiyev, A.; Dunayev, P.; Galtseva, O.; Senina, Y. Influence of Quantum Effects on Dielectric Relaxation in Functional Electrical and Electric Energy Elements Based on Proton Semiconductors and Dielectrics. *Appl. Sci.* **2023**, *13*, 8755. https://doi.org/10.3390/app13158755

Academic Editor: Antonio Vettoliere

Received: 13 June 2023
Revised: 24 July 2023
Accepted: 25 July 2023
Published: 28 July 2023

Keywords: hydrogen-bonded crystals (HBC); proton semiconductors and dielectrics (PSD); quantum diffusion polarization; quantum transparency of the potential barrier for protons in HBC; kinetic equation of dielectric relaxation (equation of transfer of relaxers by an electric field); thermally stimulated depolarization currents (TSDC); thermally stimulated depolarization currents density spectrum (TSDC-density spectrum); phenomenological Bucci–Rive formula for the TSDC density; low-temperature quantum proton relaxation (tunneling polarization); high-temperature dielectric relaxation (nonlinear volume–charge polarization); natural phlogopite; talc of Onotscoye deposit (onot talc); muscovite; chemically pure chalcanthite; the minimizing comparison function method (MCF method)

1. Introduction

The development and receiving of materials with desired properties is an important task in condensed matter physics and physical materials' science, in which hydrogen-bonded crystals (HBC) have been widely used in radio electronics, optoelectronics, and laser technology over the past two decades [1,2].

Based on the results of precision measurements of the temperature spectra of thermally stimulated depolarization currents (TSDC) in HBC, using the example of crystals of natural phlogopite $KMg_3(AlSi_3O_{10})(OH)_2$, muscovite $KAl_2(AlSi_3O_{10})(OH)_2$, onot talc $Mg_3(Si_4O_{10})(OH)_2$ chemically pure chalcanthite $CuSO_4 \cdot 5H_2O$, at temperatures above 50–550 K and polarizing field strengths of 0.1–1 MV/m, as a rule, 6–7 monorelaxation maxima are found [1–4]. The physical nature of these maxima, revealed in combination with the methods of calcination (at temperatures of 373–1373 K) and doping (in solutions of HCl, HF, NH_4OH), is diverse and occurs in the temperature range (100–450 K) through the relaxation of ionization (H_3O^+, OH^-) and orientational (L, D) Bjerrum defects, as well as the rotations of H_2O in an electric field, with different relaxer activation energies (0.1–0.7 eV) [4].

Of particular scientific interest is the low-temperature (50–100 K) maximum of TSDC density in HBC, shown by the low activation energies of relaxers (0.01–0.1 eV) [1,5]. The temperature position of this maximum in the experiment varies slightly, and the amplitude significantly depends on the concentrations of alloying impurities [4]. When crystals are calcined at temperatures of 873–1373 K, this maximum completely disappears [4]. These circumstances allow for us to assert that the physical nature of this low-temperature maximum significantly differs from the high-temperature maxima (100–450 K) and is caused by the quantum tunneling transitions of protons inside and between the ions of the anionic sublattice in the HBC [1,5,6]. Then, low-temperature, thermally stimulated depolarization in HBC can be defined as nonlinear quantum proton relaxation caused by the heating of the crystal in the absence of an external electric field [7,8]. This effect opens up the possibility of applying the quantum theory of proton conduction [1,5] to the study of nonlinear properties and the development of resonant tunnel diodes and quantum field-effect transistors based on thin films of composite materials (MIS, MSM structures) consisting of HBC-class crystals [9–15]. From this point of view, the memory elements of high-speed, non-volatile devices (DRAM, FeRAM) based on ferroelectric HBC (or materials similar to them in terms of properties and type of crystal structure) with a rectangular hysteresis loop (triglycine sulfate (TGS), ferric salt) are promising for modern computer technology [16–28]. They are characterized by abnormally high residual polarizations and long relaxation times (from 5 to 10 years), as well as a high thermal stability and mechanical strength [29–44].

The quantum theory of proton conduction and relaxation [1,5], due to the universality and generality of mathematical models, will simplify the methodology for studying the mechanisms of formation of the spontaneous polarization of ferroelectric HBC from the perspective of protons' quantum tunneling in a hydrogen sublattice near the point of phase transition of the second kind [1]. Materials of this class (KDP, DKDP) have practical appli-

cation in nonlinear optics and laser technology as regulators of laser radiation parameters, electric gates, etc. [45–51]. Fiber-optic strain sensors based on KDP and related crystals are promising [52–54].

The high proton conductivity of HBC makes it possible to use materials of this class as solid-state electrolytes in electrochemical technologies and hydrogen energy [55–61].

From this brief review of the literature, it is obvious that the further development of theoretical methods for the study of dielectric relaxation kinetics in HBC-class crystals and their composites is relevant from the perspective of both fundamental research in the mathematical description and the modeling of relaxation polarization (depolarization) and proton conduction processes, as well as for the practical applications of proton semiconductors and dielectrics in various branches of technology. The further development of this theory, within the framework of this work, refers to the improvement in existing equations and formulas describing proton relaxation and conductivity in HBC [1–8] by more strictly considering the effects of the characteristic parameters of the crystal structure and the parameters of external perturbation in formulas on the statistically averaged quantum transparency of a potential barrier perturbed by an electric field. To this end, we will take the previously built schemes of quasi-classical calculations of quantum transparency as a basis for the relaxers (protons), supplemented by mathematical elements that are important in terms of the physics of these processes. These elements will be introduced to the design formulas due to their low external disturbance in comparison with the internal crystalline potential. Previously, these elements were not taken into account in expressions regarding the quantum transparency of the parabolic potential barrier [5–7]. We will also propose a generalized non-linear solution of the quasi-classical kinetic equation of dielectric relaxation [1,6] for a small parameter of the perturbation theory. Solutions to this equation will be investigated for their polarization and depolarization processes. For the first time, we will analyze the Bucci–Rive formula, and when calculating the density of the thermally stimulated depolarization current (TSDC), relaxation times will be calculated by considering additional corrections to the rate of probability of the quantum transitions of protons through the parabolic potential barrier due to external perturbations. Previously, these amendments were not taken into account [1,6]. Note that the choice of the parabolic form of the potential barrier brings the mathematical model of relaxation polarization closer to the real spatial structure of the crystal lattice, and the results of numerical calculations of the relaxer parameters (activation energy, equilibrium concentration) and TSDC density maxima parameters should be closer to their experimental values than they were for the previously studied model of the rectangular potential barrier for protons [1,4].

2. Materials and Methods (Theoretical Bases and Methods)

The methods of the quasi-classical theory of dielectric relaxation [1,4] make it possible to accept a hydrogen ion (proton) as a physical relaxer, whose motion with different values of molecular parameters (activation energy U_0; natural oscillation frequency ν_0; potential barrier width δ_0; lattice constant a; equilibrium concentration n_0) in the vicinity (on the set of points of the continuum measure) of the temperatures of the corresponding monorelaxation maxima determines the features of thermally stimulated depolarization in various temperature ranges [1,2,4]. This approach makes it possible to classify HBC by its electrophysical properties in a wide range of field parameters (0.1–1 MV/m) and temperatures (50–550 K), as proton semiconductors and dielectrics (PSD) [1,3,4].

Theoretical studies carried out using the phenomenological theory of dielectric relaxation [1,4] point to the classical mechanism of relaxation polarization caused by the thermal activation of protons in the HBC at high temperatures (100–450 K). The calculations of the parameters of relaxers successfully correspond to their measured values in the region of high-temperature maxima of thermally stimulated depolarization currents (TSDC) [1,4].

In the low-temperature range (50–100 K), the activation energies and equilibrium proton concentrations in HBC, calculated according to the classical theory, differ markedly (by 20–50%) [1] from the values calculated from an analysis of the experimental spectra

of thermally stimulated depolarization currents (TSDC) [1,4]. This indicates the need to more strictly consider the quantum effects (associated with proton-tunneling transitions) on the theoretical TSDC density spectra in the nitrogen temperature region. This approach is further justified in the region of ultra-low temperatures (1–10 K), when the dimensional effects associated with a high probability of the quantum transition of protons inside clusters of nanometer size (1–10 nm) are manifested in HBC [1].

Recent theoretical studies have shown that the tunnel transitions of protons continue to influence the dielectric relaxation in HBC in the region of sufficiently high temperatures (250–550 K) during the formation of nonlinear space-charge polarization [1,3,7,8].

The aim of this paper is to improve the existing phenomenological theory of dielectric relaxation in HBC [1,4] by extending it to the low-temperature region (50–100 K). On this basis, a mathematical substantiation of the features of low-temperature thermally stimulated depolarization was revealed in the experiment, associated with quantum proton transitions through hydrogen bonds against the background of small activation energies and the width of the potential when the statistically averaged transparency of the potential barrier for protons reaches relatively high values. The Bucci–Rive method [1,4] will be used as the experimental methodological basis of the study, and the theoretical methodology of the study will be based on solutions of the kinetic equation describing proton transport in a potential field of a crystal lattice when disturbed by an external field, with potential parabolic barriers [1,3,7].

Based on this goal, the following research objectives were formulated:

1. Use a more stringent account of the effects that the external electric field corrections had on the statistically averaged non-stationary quantum transparency of the parabolic potential barrier for relaxers (protons) in HBC compared to previous studies [1–6]. This kind of correction for a parabolic potential barrier was not previously calculated.
2. Write a generalized solution of the quasi-classical kinetic equation of nonlinear dielectric relaxation using a small parameter of perturbation theory in HBC [1,6]. As a geometric model of the undisturbed crystalline potential, we assumed a double symmetrical potential pit with a barrier of parabolic shape. The kinetic coefficients of the kinetic equation must be calculated, considering additional elements in the expression of the quantum transparency of a potential barrier perturbed by a polarizing field. These elements were not previously calculated for the parabolic potential barrier [6]. Solutions to the generalized kinetic equation for an external field-perturbed double-symmetric potential well of parabolic form have also not been presented to date.
3. Investigate the phenomenological Bucci–Rive formula for calculating the current density of thermally stimulated depolarization (TSDC), considering additional corrections due to the external electric field and rate of probability of quantum proton transitions through the parabolic potential barrier (for initial polarization). These amendments for the parabolic potential barrier have not been calculated to date. Note that the barrier's parabolic form brings the mathematical model closer to the real spatial structure of the crystal lattice.
4. Analyze the temperature spectra of the thermally stimulated depolarization current density (TSDC) measured by the authors [1,4] for crystals of the HBC class using the example of phlogopite mica, onot talc and muscovite. Identify the physical nature of each experimental maximum and reflect the effect of crystal structure parameters and relaxer parameters (activation energy, equilibrium concentration) on the temperature, position and amplitude of TSDC mono-relaxation maxima.
5. Perform precision measurements of TSCD density temperature spectra for chalcanthite crystals. Analyze the effects of alloying impurities' concentrations and calcination temperatures on the properties and parameters of individual experimental maxima in the TSDC chalcanthite spectrum. No studies have been conducted on the density spectra of TSDC chalcanthite to date.
6. Calculate theoretical TSDC spectra for phlogopite, onot talc, muscovite and chemically pure chalcanthite crystals. Establish the nature of the effects of the design values of

the relaxer parameters on the temperature position and amplitude of each individual theoretical maximum in the TSDC density spectrum. Previously, no theoretical TSDC density spectra were calculated for the crystal potential model as a double-symmetric potential well of parabolic shape.

7. Perform numerical calculations of the parameters of relaxers (activation energy, equilibrium concentration), based on the minimizing comparison function method (MCF-method) [1]. Calculations of relaxer parameters will be carried out over a wide temperature range (50–550 K) and external field parameters (0.1–1 MV/m).
8. Investigate the effects of tunnel-proton transitions on the low-temperature (50–100 K) and high-temperature (250–550 K) TSDC density maxima properties and relaxer parameters in HBC. Studies on this level of patterns for the double-symmetric parabolic potential pit model have not been conducted to date.
9. Describe, in the form of chemical equations, the physical mechanism of quantum tunnel proton motion in HBC with a complex crystal structure (layered silicates; crystalline hydrates).

To simplify the solution to the kinetic equation, when describing the internal crystal field, we used a double-symmetric potential well [1,6], which makes it possible to exclude the influence of spatial inhomogeneities in the electric field induced by the dielectric on the kinetics of polarization. Since this paper focuses on the study of proton-tunneling mechanisms and their effect on the contours of theoretical current density graphs, rather than providing a detailed analysis of the electret effect [1], this approach is justified from a physical point of view. The crystal potential relief for protons in HBC is assumed to be one-dimensional $U_C(x)$, where x is the proton coordinate [1]. The effect of proton–proton interactions (due to the low equilibrium concentration of protons $n_0 \approx 10^{16} \div 10^{18}{}_M{}^{-3}$) and proton–phonon interactions (due to the low oscillation frequencies of anions in comparison with protons $\frac{\nu_{0,anion}}{\nu_{0,proton}} \approx 10^{-4} \div 10^{-3}$) is not taken into account, and the motion of protons is considered against the background of a static anionic subsystem [1,7].

Let us preliminarily note the fundamental formulas of the quasi-classical theory of dielectric relaxation in HBC [1,2,6,7].

The energy spectrum E of the main charge-carrier (protons) in HBC in the quasi-classical model is assumed to be quasi-continuous [1,2,7].

The one-dimensional potential barrier for the proton in HBC is assumed to be parabolic $U(x) = U_0\left(1 - \frac{4x^2}{\delta_0^2}\right)$, where δ_0 denotes the potential barrier width and U_0 denotes the activation energy.

Calculated by the WKB method, the quantum transparency of a parabolic potential barrier (1) unperturbed by an external field is $D^{(0)}(E) = \exp\left(-\frac{\pi\delta_0\sqrt{m}(U_0-E)}{\hbar\sqrt{2U_0}}\right)$. Here, m and E denote the mass and energy of the relaxer (proton), respectively.

The transparency of the unperturbed parabolic potential barrier, averaged using the quantum canonical Gibbs distribution, is the continuous function of the crystal temperature [1,2,6,7]

$$D_{quant,tunn}^{q.-classic;(0)}(T) = \langle D^{(0)}(E)\rangle = \frac{1}{k_B T}\int_0^{U_0} \exp\left(-\frac{E}{k_B T}\right) \times D^{(0)}(E)dE = \frac{\exp(-\Lambda) - \exp(-X)}{1 - \frac{\Lambda}{X}}$$

Here, the dimensionless parameters $X = \frac{U_0}{k_B T}$, $\Lambda = \frac{\pi\delta_0\sqrt{mU_0}}{\hbar\sqrt{2}}$ are calculated as functions of the molecular parameters δ_0, U_0.

From the condition $X = \Lambda$, we calculate, for the parabolic potential barrier (2), the critical temperature $T_{cr} = \frac{2}{\pi k_B}\sqrt{\frac{\hbar^2 U_0}{2m\delta_0^2}}$, below which $T < T_{cr}$, the dominant contribution to dielectric relaxation is made by the proton-tunneling inside and between ions of the anionic sublattice (quantum relaxation). At the temperatures $T > T_{cr}$ relaxation is determined by thermally activated proton transitions (thermal activation) [2,3].

Let us proceed to the study of additional properties to the temperature dependences indicated above $D^{q.-classic;(0)}_{quant,tunn}(\mathrm{T})$.

The expression $D^{q.-classic;(0)}_{quant,tunn}(\mathrm{T})$ can be used to calculate, and statistically average using the energy levels of the quasi-continuous spectrum, the probability of the protons quantum tunneling (quantum transfer) in the experimental temperature range in the vicinity of the maximum thermally stimulated depolarization currents' (TSDCs) density spectrum $\mathrm{P}_{tunn}(\mathrm{T}) = \frac{\exp(-\Lambda)-\exp(-\mathrm{X})}{1-\frac{\Lambda}{\mathrm{X}}}$. It is not difficult to see the identity $\frac{\Lambda}{\mathrm{X}} = \frac{\mathrm{T}}{\mathrm{T}_{cr}}$.

Thermal activation probability was calculated with the help of formula $\mathrm{P}_{therm}(\mathrm{T}) = \exp\left(-\frac{\mathrm{U}_0}{\mathrm{k_B T}}\right)$ [1,2,6,7].

According to the experimental data, the width of the potential barrier in HBC varies within $\delta_0 \approx 0.085 \div 0.1$ nm [1]. The experimental activation energy of protons in HBC varies from 0.01 to 0.7 eV [1].

In order to extend the theoretical range of activation energy variation, we accept this parameter within $\mathrm{U}_0 = (0.01 \div 1)$ eV.

At low temperatures, when $\mathrm{T} \ll \mathrm{T}_{cr}$ and $\Lambda \ll \mathrm{X}$, according to $\frac{1}{1-\frac{\Lambda}{\mathrm{X}}} \approx 1 + \frac{\Lambda}{\mathrm{X}}$, we have $D^{q.-classic;(0)}_{quant,tunn}(\mathrm{T}) \approx \left(1 + \frac{\Lambda}{\mathrm{X}}\right)\exp(-\Lambda)$.

Near the temperature of absolute zero, the kinetics of migratory polarization in HBC are only determined by the parameters of the potential pattern and are practically independent of temperature $D^{q.-classic;(0)}_{quant,tunn}(0) = \exp(-\Lambda)$.

With $\mathrm{T} = \mathrm{T}_{cr}$, taking $\mathrm{X} \to \Lambda$, we have $D^{q.-classic;(0)}_{quant,tunn}(\mathrm{T}_{cr}) = \Lambda\exp(-\Lambda)$.

The point of intersection of function graphs $D^{q.-classic;(0)}_{quant,tunn}(\mathrm{T})$, $D^{classic;(0)}_{therm}(\mathrm{T}) = \exp\left(-\frac{\mathrm{U}_0}{\mathrm{k_B T}}\right)$, calculated from the equation $\left(2 + \frac{\Lambda}{\mathrm{X}}\right)\exp(-\mathrm{X}) = \exp(-\Lambda)$, indicates temperature $\mathrm{T}_c > \mathrm{T}_{cr}$.

The maximum point of the functions $D^{q.-classic;(0)}_{quant,tunn}(\mathrm{T})$, calculated from the following equation

$$\mathrm{X}^2\left(\frac{\Lambda}{\mathrm{X}}\left(1 + \frac{1}{\mathrm{X}}\right) - 1\right)\exp(-\mathrm{X}) = \Lambda\exp(-\Lambda),$$

indicates temperature $\mathrm{T}_{\max} > \mathrm{T}_c$. Here, $\Lambda = -\ln\left(D^{q.-classic;(0)}_{quant,tunn}(0)\right)$.

Thus, the conditions are met:

$$\mathrm{T}_{cr} < \mathrm{T}_c < \mathrm{T}_{\max};\ D^{q.-classic;(0)}_{quant,tunn}(\mathrm{T}_{cr}) < D^{q.-classic;(0)}_{quant,tunn}(\mathrm{T}_c) < D^{q.-classic;(0)}_{quant,tunn}(\mathrm{T}_{\max}).$$

Obviously, at $\mathrm{T} \to \infty$, $D^{q.-classic;(0)}_{quant,tunn}(\mathrm{T}) \to 0$.

The behavior of the function $D^{classic;(0)}_{therm}(\mathrm{T})$ corresponds to the classical statistical theory.

The quasi-classical probability rate of proton transfer through the unperturbed potential barrier is determined considering both thermal activation and tunneling [1,7]

$$W^{q.-classic;(0)}(\mathrm{T}) = \frac{\nu_0}{2}\left(\exp(-\mathrm{X}) + D^{q.-classic;(0)}_{quant,tunn}(\mathrm{T})\right) = \frac{\nu_0}{2}\cdot\frac{\exp(-\Lambda) - \frac{\Lambda}{\mathrm{X}}\exp(-\mathrm{X})}{1-\frac{\Lambda}{\mathrm{X}}} \quad (1)$$

Here, ν_0 denotes the natural frequency of oscillations in the proton in a potential well.

In the temperature area $\mathrm{T} \ll \mathrm{T}_{cr}$, Equation (1) is converted as follows:

$$W^{q.-classic;(0)}(\mathrm{T}) \approx \ W^{q.-classic;(0)}_{quant,tunn} = \frac{\nu_0}{2} \times \frac{\exp(-\Lambda) - \exp(-\mathrm{X})}{1-\frac{\Lambda}{\mathrm{X}}}. \quad (2)$$

In the temperature area $\mathrm{T} \gg \mathrm{T}_{cr}$, Equation (1) is converted as follows:

$$W^{q.-classic;(0)}(\mathrm{T}) \approx W^{classic;(0)}_{therm} = \frac{\nu_0}{2} \times \exp(-\mathrm{X}). \quad (3)$$

Within the model of parabolic potential, between parameters δ_0 and U_0, there is an obvious communication $U_0 = \frac{m\omega_0^2\delta_0^2}{8}$. Taking the energy spectrum of the proton $E_n^{(0)} = \hbar\omega_0\left(n + \frac{1}{2}\right)$ as quasi-continuous $\left|E_{n\pm1}^{(0)} - E_n^{(0)}\right| = \hbar\omega_0 \gg k_BT$, write down the condition for the quasi-classicity of proton motion in HBC $\frac{U_0}{E_0^{(0)}} = \frac{m\omega_0\delta_0^2}{4\hbar} \gg 1$. Here, $\omega_0 = 2\pi\nu_0$.

The analysis of Equations (1)–(3) shows that, for any type of relaxation, the value of the critical temperature calculated for a rectangular barrier is 78.5% of the critical temperature in the parabolic barrier model.

From the above comparison, it is obvious that the model of a parabolic pattern in the physical sense, in contrast to the model of a rectangular pattern, is closer to the real process of the migration of structural defects and can be used in a more rigorous calculation of the theoretical spectra of thermally stimulated depolarization currents in layered crystals.

Taking the increment in the potential energy of the proton in the electric field $E(t) = E_0e^{i\omega t}$ in the approximation of a weak field inhomogeneity at distances of the order of the lattice constant $|\Delta U(t)| = \frac{1}{6}q\delta_0(\varepsilon_\infty + 2)E_0e^{i\omega t}$ [7], where ε_∞ is the permittivity associated with inductive polarization and ion charge, we write:

$$W^{q.-classic;(\pm)}(t) = \frac{\nu_0}{2}\left(\exp\left(-\frac{U_0 \pm |\Delta U(t)|}{k_BT}\right) + D_{quant,tunn}^{q.-classic;(\pm)}(t)\right) \quad (4)$$

The quantum transparency of a parabolic potential barrier perturbed by an external electric field will be calculated in the approximation $\frac{|\Delta U|}{U_0} << 1$ [7] for a proton moving with potential energy $|\Delta U(t)|$ in this direction, either along the field $D_{quant,tunn}^{q.-classic;(-)}(U_0 - |\Delta U(t)|; E)$ or against the field $D_{quant,tunn}^{q.-classic;(+)}(U_0 + |\Delta U(t)|; E)$. In [1,2], this kind of calculation was performed for a rectangular potential barrier. In this case, the choice of the parabolic form of the potential barrier allowed, at the theoretical level, for the mathematical model to be brought closer to the re-spatial structure of the crystal potential field. Then,

$$D^{(\pm)}(E) = \exp\left(-\frac{\pi\delta_0\sqrt{m}(U_0 \pm |\Delta U(t)| - E)}{\hbar\sqrt{2U_0}}\right) \quad (5)$$

Unlike earlier works [1,2,7], in this article, the statistical averaging of non-stationary quantum transparency will be carried out with a stricter consideration of the effects of the corrections $\xi(t) = \left|\frac{\Delta U(t)}{k_BT}\right|$, $\eta(t) = \Lambda\left|\frac{\Delta U(t)}{U_0}\right|$ due to the electric field. To create a parabolic potential barrier, these transformations will be completed for the first time. Then, based on

$$D_{quant,tunn}^{q.-classic;(\pm)}(t) = \frac{1}{k_BT}\int_{2|\Delta U(t)|,0}^{U_0\pm|\Delta U(t)|} \exp\left(-\frac{E}{k_BT}\right) \times D^{(\pm)}(U_0 \pm |\Delta U(t)|; E)dE \quad (6)$$

and considering Equation (5), we obtain

$$D_{quant,tunn}^{q.-classic;(+)}(t) = \frac{\exp(-\Lambda)\exp(\eta(t))\exp(-2\xi(t)) - \exp(-X)\exp(-\xi(t))}{1 - \frac{\Lambda}{X}} \quad (7)$$

$$D_{quant,tunn}^{q.-classic;(-)} = \frac{\exp(-\Lambda)\exp(\eta(t)) - \exp(-X)\exp(\xi(t))}{1 - \frac{\Lambda}{X}} \quad (8)$$

Calculating the kinetic coefficients leads to:

$$\Omega^{(\omega)}(t) = \frac{W^{q.-classic;(-)}(t) + W^{q.-classic;(+)}(t)}{2} =$$
$$= \frac{\nu_0}{2}\left(\exp(-X)ch(\xi(t)) + \frac{\frac{1}{2}\exp(-\Lambda)\exp(\eta(t))(1+\exp(-2\xi(t))) - \exp(-X)ch(\xi(t))}{1-\frac{\Lambda}{X}}\right), \quad (9)$$

$$\Xi^{(\omega)}(t) = W^{q.-classic;(-)}(t) - W^{q.-classic;(+)}(t) = \\ = \nu_0\left(\exp(-X)\mathrm{sh}(\xi(t)) + \frac{\frac{1}{2}\exp(-\Lambda)\exp(\eta(t))(1-\exp(-2\xi(t)))-\exp(-X)\mathrm{sh}(\xi(t))}{1-\frac{\Lambda}{X}}\right), \quad (10)$$

Here, ω is the cyclic frequency of the external field.

In this case, the relation $\frac{\eta(t)}{\xi(t)} = \frac{\Lambda}{X} = \frac{T}{T_{cr}}$, which is important for the quasi-classical model, is fulfilled.

In Equations (9) and (10), in addition to [1,2,7] elements, $\frac{1}{2}\exp(\eta(t)) \times (1 \pm \exp(-2\xi(t)))$ indicates the influence of external indignation in the form of correction parameters $\xi(t) = \left|\frac{\Delta U(t)}{k_B T}\right|$, $\eta(t) = \Lambda\left|\frac{\Delta U(t)}{U_0}\right|$ on non-stationary kinetic coefficients $\Omega^{(\omega)}(t)$, $\Xi^{(\omega)}(t)$. Earlier, such amendments were not taken into account. Their consideration in these functions will make it possible to more strictly assess the influence of the external electric field on the solutions of the kinetic equation and, accordingly, polarization.

The study of dielectric relaxation in layered dielectrics uses the solution of the kinetic equation [6]:

$$\frac{d\Delta n^{(\omega)}(t)}{dt} + 2\Omega^{(\omega)}(t)\Delta n^{(\omega)}(t) = \frac{1}{3}n_0\Xi^{(\omega)}(t) \quad (11)$$

In (11), $\Delta n^{(\omega)}(t) = \Delta n^{(\omega)}(t) - n_0$ is a concentration of relaxers (protons) in excess of the balanced concentration n_0.

No initial polarization was used: $\Delta n^{(\omega)}(0) = 0$.

Kinetic Equation (11) was built and studied in [6,8]. Moreover, Ref. [2] solved an even more physically stringent kinetic equation regarding proton (for HBC) and ion (for a wide class of dielectrics) relaxation based on a multi-pit crystal potential model. Here, we limit ourselves to a simpler kinetic equation for a dual-symmetric potential pit model, with the aim that the format of this model will qualitatively fit the Bucci–Rive thermally stimulated depolarization (TSCD) current calculation scheme described below. The disadvantage of the kinetic equation solutions we chose is that this model does not consider the heterogeneity of the electric field in the dielectric, unlike other works [1,2]. However, since we did not conduct studies on the electro-tertiary effect and the effects associated with homocharge relaxation in this manuscript, the physical severity of the final re-results is not at all reduced when choosing a more simplified kinetic Equation (11).

In addition, in this work, in continuation of that of [6], we will strengthen the influence of external perturbation parameters $\xi(t) = \left|\frac{\Delta U(t)}{k_B T}\right|$, $\eta(t) = \Lambda\left|\frac{\Delta U(t)}{U_0}\right|$ on the final solutions to Equation (11). To this end, solutions of Equation (11) must be written using perturbation theory methods, allowing for their decomposition into infinite power series by degrees of perturbation parameters $\xi(t)$ in the form:

$$\Delta n^{(\omega)}(t) = \sum_{s=1}^{\infty}\xi_0^s\Delta\left(\Delta n^{(\omega)}(t)\right)^{(s)}, \\ \Omega^{(\omega)}(t) = \sum_{l=0}^{\infty}\sum_{p=0}^{\infty}(\xi(t))^l(\eta(t))^p\left(\Omega^{(\omega)}(t)\right)^{(l,p)}, \\ \Xi^{(\omega)}(t) = \sum_{l=0}^{\infty}\sum_{p=0}^{\infty}(\xi(t))^l(\eta(t))^p\left(\Xi^{(\omega)}(t)\right)^{(l,p)}.$$

According to the relation $\frac{\eta(t)}{\xi(t)} = \frac{T}{T_{cr}}$, the auxiliary identities hold.

$$(\xi(t))^l(\eta(t))^p = (\xi(t))^{l+p} \times \left(\frac{T}{T_{cr}}\right)^p, \ (\xi(t))^l(\eta(t))^p = (\eta(t))^{p+l} \times \left(\frac{T_{cr}}{T}\right)^l.$$

Elements of series $\left(\Omega^{(\omega)}(t)\right)^{(s)}$, $\left(\Xi^{(\omega)}(t)\right)^{(p)}$ follow from Equations (9) and (10).

This method is effective in the construction of solutions to Equation (11) for the processes of dielectric losses when the electric field is variable and the parameters $\xi(t)$, $\eta(t)$ are considered only as functions of time. This work examines the process of thermally

stimulated depolarization; therefore, there is no strict need to apply perturbation theory methods and the work can be limited to other, more mathematically simple methods, which are set out below. However, it should be noted that the methods of perturbation theory are the solutions of Equation (11).

Without limiting the generality of the results, let us write the solution of Equation (11) through a linear approximation using the small dimensionless parameters $\xi(t) = \xi_0 \exp(i\omega t)$, $\eta(t) = \eta_0 \exp(i\omega t)$, where $\xi_0 = \left|\frac{(\Delta U)_0}{k_B T}\right|$, $\eta_0 = \Lambda\left|\frac{(\Delta U)_0}{U_0}\right|$, $(\Delta U)_0 = \frac{1}{6} q \delta_0 (\varepsilon_\infty + 2) E_0$. Then, using the approximate expressions

$$\Delta n^{(\omega)}(t) = \xi_0 \left(\Delta n^{(\omega)}(t)\right)^{(1)},$$
$$\Omega^{(\omega)}(t) \approx \frac{\nu_0}{2}\left(\exp(-X) + \frac{\exp(-\Lambda) - \exp(-X)}{1 - \frac{\Lambda}{X}}\right) = W^{q.-classic;(0)},$$
$$\Xi^{(\omega)}(t) \approx \nu_0\left(\exp(-X) + \frac{\exp(-\Lambda) - \exp(-X)}{1 - \frac{\Lambda}{X}}\right) \times \xi(t) = 2W^{q.-classic;(0)} \times \xi_0 \exp(i\omega t),$$

set up the equation:

$$\frac{d\left(\Delta n^{(\omega)}(t)\right)^{(1)}}{dt} + 2W^{q.-classic;(0)}\left(\Delta n^{(\omega)}(t)\right)^{(1)} = \frac{2}{3} n_0 W^{q.-classic;(0)} \times \exp(i\omega t). \quad (12)$$

Its solution, taking into account $\left(\Delta n^{(\omega)}(0)\right)^{(1)} = 0$, describes transient processes in the dielectric

$$\left(\Delta n^{(\omega)}(t)\right)^{(1)} = \frac{2}{3} \times \frac{n_0 W^{q.-classic;(0)}}{i\omega + 2W^{q.-classic;(0)}}\left(\exp(i\omega t) - \exp\left(-2W^{q.-classic;(0)} t\right)\right). \quad (13)$$

In the stationary polarization mode, we have

$$\Delta n^{(\omega)}(t) = \frac{1}{9} \times \frac{n_0 W^{(0)} q \delta_0 (\varepsilon_\infty + 2) E_0}{\left(i\omega + 2W^{(0)}\right) k_B T} \exp(i\omega t). \quad (14)$$

When $\omega = 0$, we obtain

$$\Delta n^{(\omega=0)}(t) = \frac{1}{18} \times \frac{n_0 q \delta_0 (\varepsilon_\infty + 2) E_0}{k_B T}. \quad (15)$$

The system relaxation time $\tau^{(\omega)}(t) = \frac{1}{2\Omega^{(\omega)}(t)}$ in the accepted approximation is $\tau^{(\omega)}(t) \approx \frac{1}{2W^{q.-classic;(0)}(T)}$.

The solution of the kinetic Equation (11) in the form of Equations (12) and (13) is applicable in the region of weak fields $\xi(t) \ll 1$, $\eta(t) \ll 1$.

To more strictly take into account the influence of the external perturbance parameters ξ(t), η(t) on the polarization of the dielectric, it is necessary to construct a generalized solution to the nonlinear kinetic equation. This approach is effective in the region of anomalously high-polarization nonlinearities, which manifest themselves in HBC in the region of ultralow temperatures (1–10 K) in weak fields (0.1–1 MV/m), and in the region of ultrahigh temperatures (550–1500 K and higher) in strong fields (10–1000 MV/m) [1,2,7]. The theoretical investigation of the kinetics of quantum proton relaxation and conductivity near absolute zero temperatures are a rather complicated scientific problem from a physical point of view. If, formally, we have the opportunity to extend the mathematical model of the nonlinear quantum polarization in HBC in the form of Equations (9)–(11), and in the form of [1,2,5] to the temperature range T = 0–1 K, then from the point of view of the fundamental physical rigor of the final results, it is extremely difficult to assert anything

in this case. In [1,2], situations with values of the dimensionless small parameter ξ, of perturbation theory equal to ξ = 0.1–1 at temperatures T = 1–10 K are touched upon, but the model of these phenomena remains quasi-classical, and is not strictly quantum mechanical. At HBC temperatures near absolute zero, fundamentally new quantum kinetic phenomena appeared, associated with the interaction between proton and phonon subsystems similar to electronic superconductivity. However, at this time, these effects in HBC have not yet been explored, either theoretically or experimentally. Although the theoretical studies of quantum proton relaxation in nanosized HBC layers (1–10 nm) in an electric field at ultralow temperatures (4–25 K) are described in great detail in [1], in the physical sense, the mathematical model of these studies is still far from perfect. In this situation, taking into account the influences of sufficiently high values of field parameters (10–1000 MV/m) and ultra-low temperatures, we will limit the region T = 1–10 K within the framework of the non-linear quasi-classical theory of proton relaxation. In this case, to conduct a more rigorous study of the kinetic Equation (11), we write down its solution in the generalized form:

$$\Delta n^{(\omega)}(t) = \frac{1}{3} n_0 \int_0^t \Xi^{(\omega)}(t) \times \exp\left(2 \int \Omega^{(\omega)}(t) \mathrm{d}t\right) \mathrm{d}t \times \exp\left(-2 \int \Omega^{(\omega)}(t) \mathrm{d}t\right), \quad (16)$$

where the expression $\int \Omega^{(\omega)}(t) \mathrm{d}t$ means the antiderivative of the function $\Omega^{(\omega)}(t)$.

The study of the Equation (16), in a complex with Equations (9) and (10), is a problem that cannot be analytically solved, especially in the complex plane.

A numerical study of Equation (16) is a separate problem, the solution of which goes beyond the boundaries of this paper and will be determined later.

Let us move on to the case of polarization in a stationary electric field. Then, from Equation (16), we can obtain

$$\Delta n^{(\omega=0)}(t) = \frac{1}{3} n_0 \times \frac{\Xi^{(\omega=0)}}{2\Omega^{(\omega=0)}} \times \left[1 - \exp\left(-2\Omega^{(\omega=0)t}\right)\right], \quad (17)$$

where

$$\Omega^{(\omega=0)} = \Omega_{st} = \frac{\nu_0}{2}\left(\exp(-X)\mathrm{ch}(\xi_0) + \frac{\frac{1}{2}\exp(-\Lambda)\exp(\eta_0)(1+\exp(-2\xi_0)) - \exp(-X)\mathrm{ch}(\xi_0)}{1-\frac{\Lambda}{X}}\right), \quad (18)$$

$$\Xi^{(\omega=0)} = \Xi_{st} = \nu_0\left(\exp(-X)\mathrm{sh}(\xi_0) + \frac{\frac{1}{2}\exp(-\Lambda)\exp(\eta_0)(1-\exp(-2\xi_0)) - \exp(-X)\mathrm{sh}(\xi_0)}{1-\frac{\Lambda}{X}}\right). \quad (19)$$

Equation (17), a stationary non-linear function of temperature, makes it possible to study the process of thermally stimulated polarization, considering Equations (18) and (19), written as functions of temperature. The system relaxation time is given in the accepted approximation: $\tau^{(\omega)}(t) \to \tau^{(\omega=0)}(\mathrm{T}) = \tau_{st}(\mathrm{T}) = \frac{1}{2\Omega_{st}(\mathrm{T})}$.

The application of Equation (17) for the case of isothermal polarization assumes that Equations (18) and (19) are model constants, calculated at an equal temperature to the crystal polarization temperature T_{pol}. In this case, when $t \gg \tau_{st}$, the linear approximation with respect to the small parameters $\xi_0 \ll 1$, $\eta_0 \ll 1$ leads to the transformation of the $\Omega_{st} \to W^{q.-classic;(0)}$, $\Xi_{st} \to 2W^{q.-classic;(0)}\xi_0$ and Equation (17) to Equation (15) in the form $\Delta n^{(\omega=0)}(t) \to \frac{1}{3} n_0 \times \xi_0$, which is one of the criteria for the reliability of Equations (9), (10) and (16).

The results of numerical calculations are given in Equation (18). We will separately investigate temperature dependencies for stationary probabilities of a classical $D^{classic}_{term;stationary}(\mathrm{T}) = \exp(-X)\mathrm{ch}(\xi_0)$ and quantum tunnel characters on the basis of equality $D^{q.-classic}_{quant,tunn;stationary}(\mathrm{T}) = \frac{\frac{1}{2}\exp(-\Lambda)\exp(\eta_0)(1+\exp(-2\xi_0))-\exp(-X)\mathrm{ch}(\xi_0)}{1-\frac{\Lambda}{X}}$. The temperature is accepted in diapason from 0 to 2500 K. The value of the polarizing field strength is taken

as $E_0 = 10^6$ V/m. According to the results of numerical calculations, the value of the polarizing field strength has practically no effect on the values of quantum transparency $D^{q.-classic}_{quant,tunn;stationary}(T)$ in the region of fields $E_0 = \left(10^6 \div 10^7\right)$ V/m at a wide range of temperatures T = 0–2500 K, and only in the region $E_0 = \left(10^8 \div 10^9\right)$ V/m does the field begin to affect the value of quantum transparency.

According to the results of numerical calculations, at the activation energy of $U_{01} = 0.01$ eV, when the characteristic parameter is $\Lambda_1 = \frac{\pi\delta_0\sqrt{mU_{01}}}{\hbar\sqrt{2}} = X_{cr,1} = \frac{U_{01}}{k_B T_{cr,1}} \approx 2.921406892621811$, the critical temperature of $T_{cr,1} = \frac{\hbar\sqrt{2U_{01}}}{\pi k_B \delta_0 \sqrt{m}} \approx 39.5774$ K, at which the stationary statistically averaged quantum transparency of the parabolic potential barrier that is perturbed by the external field is $D^{q.-classic}_{quant,tunn;stationary}(T_{cr,1}) \approx 0.1555$. Further, at the activation energy of $U_{02} = 0.03$ eV, the critical temperature is $T_{cr,2} = \frac{\hbar\sqrt{2U_{02}}}{\pi k_B \delta_0 \sqrt{m}} \approx 68.55$ K, and the corresponding stationary quantum transparency is $D^{q.-classic}_{quant,tunn;stationary}(T_{cr,2}) \approx 0.031$. At the activation energy of $U_{03} = 0.05$ eV, when the critical temperature is $T_{cr,3} \approx 88.4977$ K the stationary quantum transparency is $D^{q.-classic}_{quant,tunn;stationary}(T_{cr,3}) \approx 0.008$. Further, at the activation energy of $U_{04} = 0.07$ eV, we obtain, respectively, $T_{cr,4} \approx 104.7119$ K, $D^{q.-classic}_{quant,tunn;stationary}(T_{cr,4}) \approx 0.0035$. At an activation energy of $U_{05} = 0.1$ eV, we have $T_{cr,5} \approx 125.1546$ K, $D^{q.-classic}_{quant,tunn;stationary}(T_{cr,5}) \approx 0.00087$.

The obtained numerical results indicate that the theoretical values of the stationary quantum transparency $D^{q.-classic}_{quant,tunn;stationary}(T)$ are shifted towards higher critical temperatures T_{cr} with a decrease in the amplitude values of the quantum transparency and an increase in the energy of proton activation. Against the background of small activation energies (0.01.0.03.05, 0.07 eV), critical temperatures (39.57 K, 68.55 K, 88.49 K, 104.71 K) are distributed in the T < 105 K region with sufficiently high amplitudes of quantum transparency (0.1555, 0.031, 0.008, 0.0035) for such heavy (in comparison with electrons) charge carriers as protons. With an activation energy of 0.1 eV, the critical temperature shifts to 125.15 K, and the amplitude of the quantum transparency decreases to 0.00087. This indicates the significant contribution of quantum tunneling to the relaxation motion of protons in HBC in the temperature region T = 1–100 K. At temperatures T > 100, quantum tunneling continues to affect the relaxation of protons in HBC to a certain extent.

The phenomenological model of thermally stimulated depolarization currents proposed by Bucci-Rive [23,32], involves a study of the mechanism of thermal destruction of the polarized state established during polarization (in a uniform stationary electric field of strength $E_{pol,0}$ at polarization temperature T_{pol}) in the absence of an external electric field.

The solution of kinetic Equation (11) for the process of thermally stimulated depolarization in the absence of an external electric field, when the equation $\frac{d\Delta n_{depol}(t)}{dt} + \frac{\Delta n_{depol}(t)}{\tau_{depol}} = 0$, considering the initial condition $\Delta n_{depol}(0) = \Delta n_{pol}^{(\omega=0)}(\infty)$, takes the form $\Delta n_{depol}(t) = \Delta n_{pol} \times \exp\left(-2\int_0^t \Omega_{depol}(T)dt\right)$. The advantage of this expression for excessive proton concentration in the thermally stimulated depolarization formulated in this article is as follows. First, in [4,8], the calculation of the function $\Delta n_{depol}(t)$ is constructed considering the effects of quantum tunneling on the statistically averaged transparency of the parabolic potential barrier, which is reflected in the expression for $\Omega_{depol}(T)$. Previously, no studies of this kind have been conducted for the potential barrier of the parabolic form. Moreover, the parabolic potential barrier model is physically closer to the structure and properties of the real crystal lattice than the rectangular potential barrier model [4]. Secondly, unlike [8], the calculation of the excess concentration of protons $\Delta n_{pol} = \Delta n_{pol}^{(\omega=0)}(\infty) = \frac{1}{3} n_0 \times \frac{\Xi_{st}(T_{pol})}{2\Omega_{st}(T_{pol})}$ established during polarization is carried out by us in Equation (17), by taking into account the effects of additional correction elements элементов $\frac{1}{2}\exp(\eta_0) \times (1 \pm \exp(-2\xi_0))$ on non-stationary kinetic coefficients

Ω_{st}, Ξ_{st} (18) and (19). This technique increases, at a theoretical level, the contribution to the polarization of the dielectric caused by the external field of nonlinearities.

The rate of proton transition probabilities at thermally stimulated depolarization, according t0 Equation (9), at the $\xi(t) = 0$, $\eta(t) = 0$, takes the form

$$\Omega_{\text{depol}}(\mathrm{T}) = W^{q.-classic;(0)}(\mathrm{T}) = \frac{\nu_0}{2}\left(\exp(-\mathrm{X}) + \frac{\exp(-\Lambda) - \exp(-\mathrm{X})}{1 - \frac{\Lambda}{\mathrm{X}}}\right). \quad (20)$$

The relaxation time of the ions for the process of thermally stimulated depolarization is $\tau_{\text{depol}}(\mathrm{T}) = \frac{1}{2\Omega_{\text{depol}}(\mathrm{T})}$.

The increase in the concentration of relaxers during thermally stimulated depolarization becomes a function of temperature. For an arbitrary nonlinear law of heating with a rate $\mathrm{c}(\mathrm{T}) = \frac{\mathrm{dT}}{\mathrm{d}t}$, we have

$$\Delta n_{\text{depol}}(\mathrm{T}) = \Delta n_{\text{pol}} \times \exp\left(-2\int_{\mathrm{T}_0}^{\mathrm{T}} \frac{\Omega_{\text{depol}}(\mathrm{T})\mathrm{dT}}{\mathrm{c}(\mathrm{T}))}\right). \quad (21)$$

Thermally stimulated depolarization current density $\mathrm{j}_{\text{depol}}(t) = -\frac{\partial P_{\text{depol}}(t)}{\partial t}$, calculated on the basis of $P_{\text{depol}}(t) = \frac{1}{2}\mathrm{q}\delta_0 \times \Delta n_{\text{depol}}(t)$ according to the Bucci–Rive theory [7], in the case of heating of the crystal according to the linear law $\mathrm{c} = \frac{\mathrm{dT}}{\mathrm{d}t} = const$, takes the form

$$\mathrm{j}_{\text{depol}}(\mathrm{T}) = \mathrm{q}\delta_0 \times \Delta n_{pol} \times \Omega_{\text{depol}}(\mathrm{T}) \times \exp\left(-\frac{2}{\mathrm{c}}\int_{\mathrm{T}_0}^{\mathrm{T}} \Omega_{\text{depol}}(\mathrm{T})\mathrm{dT}\right). \quad (22)$$

The study of the integral $\int_{\mathrm{T}_0}^{\mathrm{T}} \Omega_{\text{depol}}(\mathrm{T})\mathrm{dT}$ with the integrand $\Omega_{\text{depol}}(\mathrm{T})$ was carried out by numerical methods.

The applied scientific novelty of the Equation (22), in the context of this problem, consists of a number of additional model transformations and refinements embedded in the structure of analytical expressions for calculating quantities Δn_{depol} и $\Omega_{\text{depol}}(\mathrm{T})$ that, as noted above, carries significant physical stress associated with the effects of nonlinear polarization effects on proton relaxation kinetics during polarization in HBC. The solution of these issues is relevant to the analysis of the experimental spectra of thermally stimulated dependence currents (TSDC) and in predicting the properties and parameters of functional elements of electrical installations and electronic and electronically controlled systems based on HBC with a complex crystal structure.

3. Results (A Comparison of the Theoretical and Experimental Results)

The calculation of the theoretical values of the parameters of relaxers (activation energy, balanced concentration) was carried out by computer-processing Formula (25) with the help of the minimizing the comparison function method (MCF method) [62–67], comparing the theoretical and experimental graphs of the thermally stimulated depolarization current (TSDC) density in the vicinity of each experimental monorelaxation maximum $\left(\mathrm{T}_{\text{exp,max}}, \mathrm{j}_{\text{exp,max}}\right)$ on the set of points of the continuum measure by varying the numerical values of the theoretical parameters of the set $\zeta_0 = \{\mathrm{U}_0; \delta_0; \nu_0; n_0; a\}$.

The results of the numerical calculation are shown in Tables 1–4.

The numerical values of the molecular parameters in the Tables 1–3, calculated for each type of relaxer, correspond to the experimentally measured peaks in the density spectra of thermally stimulated depolarization currents (TSDC) in Figures 1–3 for mica natural phlogopite, onot talc, and muscovite at various polarization temperatures T_{pol} and polarization field strengths $\mathrm{E}_{\text{pol},0}$. The identification of the physical nature of the first six maxima was carried out in combination with the calcination methods (in the temperature range $\mathrm{T}_{\text{calcination}}$ = 473–1373 K when adsorbed, and crystallization water was completely removed from the crystals) before doping (proton–acceptor and proton–donor impurities).

As a result, from dependencies $j_{max} = f\left(T_{pol}, E_{pol,0}, T_{calcination}\right)$, it was found that maxima 1-6 are due to dipole polarization [1,4]. The density amplitude of the TSDC in the region of the seventh maximum is nonlinearly dependent on the quantity $E_{pol,0}$. At the same time, with a decrease in T_{pol}, regardless of the temperature $T_{calcination}$, the seventh maximum shifts to the low-temperature area and can even cover the sixth maximum. At a fixed polarization temperature T_{pol}, the temperature position of the seventh maximum depends on the temperature $T_{calcination}$ of the sample [1,4]. Therefore, it can be assumed that the high-temperature maximum is due to the accumulation and resorption of charge (bulk-charge polarization). This type of polarization can be defined as interlayer polarization. In this area of temperature (300–500 K), an electric current is introduced to the dielectric.

Table 1. Relaxator parameters in natural phlogopite $KMg_3(AlSi_3O_{10})(OH)_2$, calculated using the phenomenological theory of thermally stimulated depolarization currents (TSDC) for the parabolic potential barrier model (Graph 1 in Figure 1).

Temperature of Experimental Maximum of TSDC	Type of Relaxator	Energy Activation U_0, eV			Balanced Concentration n_0, 10^{16} m^{-3}		
		Experimental [1,4]	Theoretical (Calculated Based on Equation (22))		Experimental (Calculation in This Paper)	Theoretical (Calculated Based on Equation (22)), 10^{16}	
			Without Considering the Quantum Tunneling	Considering the Quantum Tunneling		Without Considering the Quantum Tunneling	Considering the Quantum Tunneling
100	$HSiO_4^{3-}$	0.05 ± 0.01	0.12	0.06	1.4	1.5	1.4
130	H_3O^+	0.17 ± 0.02	0.19	0.18	1.3	1.33	1.29
178	H_2O water molecules of crystallization (structural water)	0.25 ± 0.03	0.27	0.27	200	208	205
206	H_2O-adsorbed water molecules (on bundles)	0.31 ± 0.03	0.32	0.32	30	32	32
235	OH^-	0.40 ± 0.04	0.42	0.41	120	122	120
257	L,D defects, VL,VD complexes	0.49 ± 0.05	0.51	0.49	200	207	205
405	H_3O^+, OH^-, H^+	0.35 ± 0.05	0.45	0.42	3500	3200	3520

Table 2. Relaxer parameters in natural mineral of onot talc $Mg_3(Si_4O_{10})(OH)_2$, calculated using the phenomenological theory of thermally stimulated depolarization currents (TSDC) for the parabolic potential barrier model (Graph 1 in Figure 2).

Temperature of Experimental Maximum of TSDC	Type of Relaxator	Energy Activation U_0, eV			Balanced Concentration n_0, 10^{16} m^{-3}		
		Experimental [1,4]	Theoretical (Calculated Based on Equation (22))		Experimental (Calculation in This Paper)	Theoretical (Calculated Based on Equation (22)), 10^{16}	
			Without Considering the Quantum Tunneling	Considering the Quantum Tunneling		Without Considering the Quantum Tunneling	Considering the Quantum Tunneling
86	$HSiO_4^{3-}$	0.06 ± 0.01	0.12	0.06	1.4	1.5	1.4
112	H_3O^+	0.09 ± 0.02	0.19	0.18	1.3	1.33	1.29
180	H_2O water molecules of crystallization (structural water)	0.19 ± 0.02	0.27	0.27	200	208	205
206	H_2O-adsorbed water molecules (on bundles)	0.25 ± 0.03	0.32	0.32	30	32	32
230	OH^-	0.32 ± 0.04	0.42	0.41	120	122	120
251	L,D defects, VL,VD complexes	0.41 ± 0.04	0.51	0.49	200	207	205
305	H_3O^+, OH^-, H^+	0.40 ± 0.06	0.49	0.43	4600	3900	4610

Table 3. Relaxer parameters in natural mineral of muscovite $KAl_2(AlSi_3O_{10})(OH)_2$, calculated using the phenomenological theory of thermally stimulated depolarization currents (TSDC) for the parabolic potential barrier model (Graph 4 in Figure 3).

Temperature of Experimental Maximum of TSDC	Type of Relaxator	Energy Activation U_0, eV			Balanced Concentration n_0, 10^{16} m^{-3}		
		Experimental (Calculation in this Paper)	Theoretical (Calculated Based on Equation (22))		Experimental (Calculation in This Paper)	Theoretical (Calculated Based on Equation (22)), 10^{16}	
			Without Considering the Quantum Tunneling	Considering the Quantum Tunneling		Without Considering the Quantum Tunneling	Considering the Quantum Tunneling
105	$HSiO_4^{3-}$	0.04 ± 0.01	0.08	0.05	1.2	1.4	1.2
153	H_3O^+	0.08 ± 0.02	0.12	0.09	1.5	1.45	1.52
190	H_2O water molecules of crystallization (structural water)	0.17 ± 0.02	0.19	0.19	240	241	240
206	H_2O-adsorbed water molecules (on bundles)	0.23 ± 0.03	0.25	0.25	34	34	34
230	OH^-	0.30 ± 0.04	0.34	0.34	127	123	127
246	L,D defects, VL,VD complexes	0.40 ± 0.04	0.44	0.44	230	228	231
295	H_3O^+, OH^-, H^+	0.38 ± 0.06	0.40	0.45	4370	4250	4350

Table 4. Relaxator parameters in chalcanthite $CuSO_4 \cdot 5H_2O$, calculated using the phenomenological theory of thermally stimulated depolarization currents (TSDC) for the parabolic potential barrier model (Graph 1 in Figure 4).

Temperature of Experimental Maximum of TSDC	Type of Relaxer	Energy Activation U_0, eV			Balanced Concentration n_0, 10^{16} m^{-3}		
		Experimental (Calculation in This Paper)	Theoretical (Calculated Based on Equation (24))		Experimental (Calculation in This Paper Carried Out by Quasi-Empirical Methods [1,4])	Theoretical (Calculated Based on Equation (24))	
			Without Considering the Quantum Tunneling	Considering the Quantum Tunneling		Without Considering the Quantum Tunneling	Considering the Quantum Tunneling
94	HSO_4^-	0.07 ± 0.01	0.16	0.08	1.8	1.7	1.79
138	H_3O^+	0.11 ± 0.01	0.13	0.12	1.5	1.6	1.52
170	H_2O water molecules of crystallization (structural water)	0.23 ± 0.02	0.26	0.25	190	185	189
206	H_2O-adsorbed water molecules (on bundles)	0.35 ± 0.03	0.37	0.37	410	410	410
230	OH^-	0.50 ± 0.05	0.54	0.54	550	530	550
246	L,D defects, VL, VD complexes	0.70 ± 0.08	0.77	0.75	2100	2000	2080
290	H_3O^+, OH^-, H^+	0.34 ± 0.04	0.41	0.35	24,734	23,128	24,572

In this article, we will not go into the experimental schemes for studying the properties and parameters of spectra (TSDC) described in [1,4].

In this paper, we studied, under various experimental conditions, the spectrum of thermally stimulated depolarization current density (TSDC) for crystals of chemically pure chalcanthite, classified by the type and properties of their crystal structure as a crystalline hydrate, which is classified by Werner as a complex compound [1]. With the experimental measuring device described in [68], we measured the main spectrum (Graph 1 in Figure 4) and a number of additional spectra (Graphs 2–5 in Figure 4), from which it was found that, in chalcanthite, as in samples of laminated silicates (phlogopite, talc, muscovite), seven

monorelaxation TSDC density maximums were found due to the silicate-like physical mechanisms of relaxation polarization [1,3].

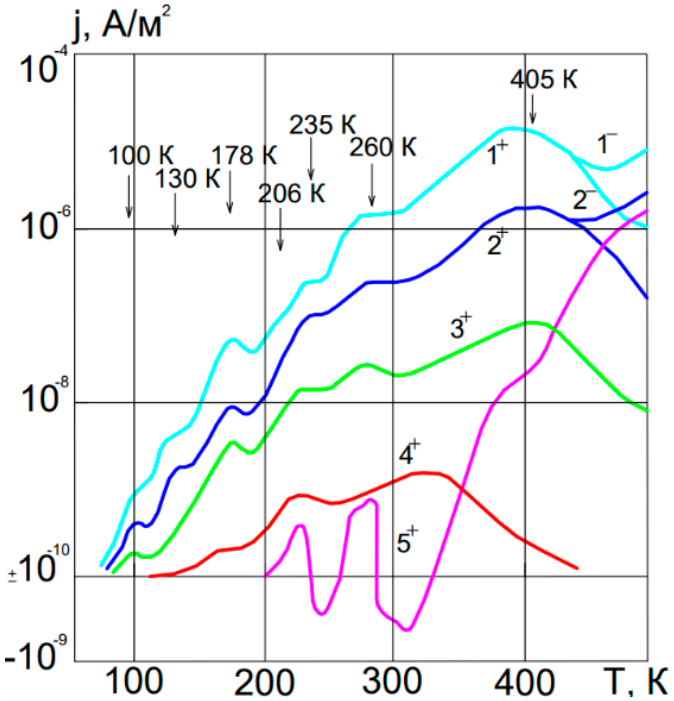

Figure 1. Phlogopite TSDC density spectrum for $E_{pol,0} = 10^6$ V × m^{-1}, T_{pol} = 373 K, d = 30 mkm: 1^+, 1^-—natural phlogopite; 2^+, 2^-, 3^+, 4^+—calcined at temperatures $T_{an,2}$ = 873 K, 3^+—$T_{an,3}$ = 1073 K, 4^+—$T_{an,4}$ = 1373 K; 5^+—density spectrum of thermally stimulated polarization current (TSPC). The sign next to the number indicates the polarity of the sample [1,4].

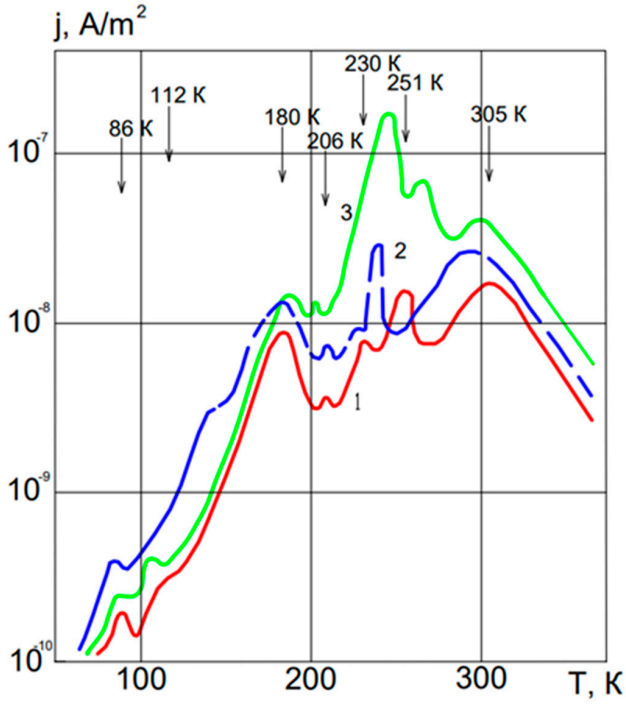

Figure 2. Thermally stimulated depolarization current density spectrum of onot talc. 1—natural mineral of onot talc $Mg_3(Si_4O_{10})(OH)_2$, 2—talc doped in hydrochloric acid solution ($n_{HCl} = 7.4 \times 10^{-5}$mol/m^3). 3—talc doped in NH_4OH solution ($n_{NH_4OH} = 9.2 \times 10^{-5}$ mol/m^3). The measurements were carried out at $E_{pol,0} = 2 \times 10^5$ V × m^{-1}, T_{pol} = 300 K, c = 0.1 K × s^{-1} [1,4].

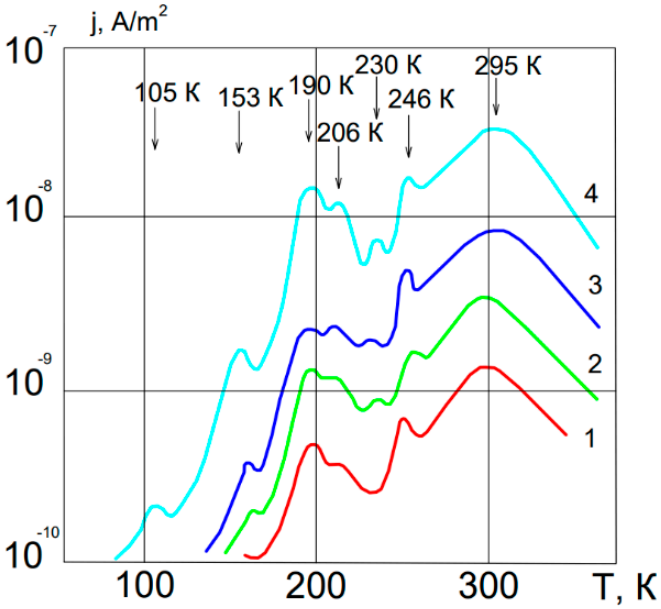

Figure 3. Thermally stimulated depolarization current density spectrum of muscovite $KAl_2(AlSi_3O_{10})(OH)_2$. 1—$E_{pol,0} = 2 \times 10^5$ V × m^{-1}, 2—$E_{pol,0} = 5 \times 10^5$ V × m^{-1}, 3—$E_{pol,0} = 10^6$ V × m^{-1}, 4—$E_{pol,0} = 5 \times 10^6$ V × m^{-1}. The measurements were carried out at T_{pol} = 300 K, t_{pol} = 15 min, c = 0.1 K × s^{-1} [1,4].

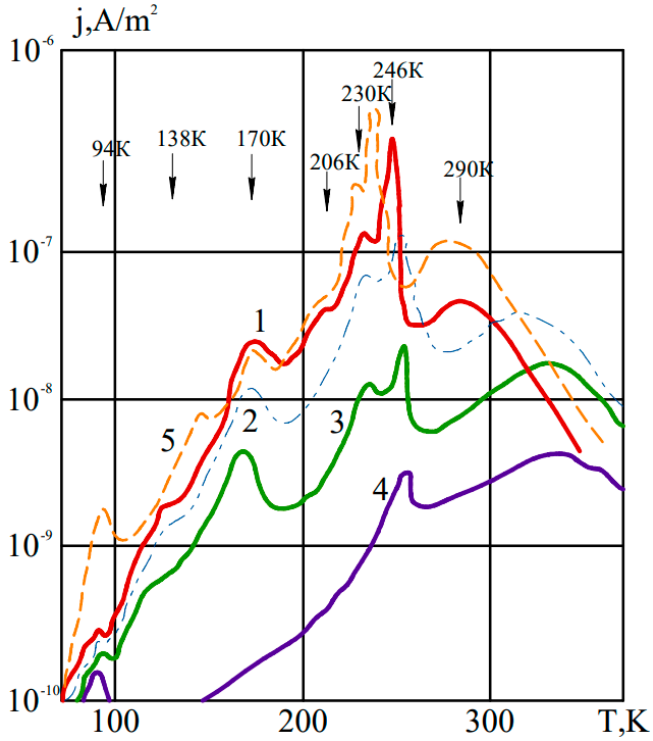

Figure 4. Thermally stimulated depolarization current density spectrum of copper sulfate. 1—$CuSO_4 \cdot 5H_2O$ (chemically pure chalcanthite), 2—$CuSO_4 \cdot 3H_2O$, 3—$CuSO_4 \cdot H_2O$, 4—$CuSO_4$ (300 °C), 5—$CuSO_4 \cdot 5H_2O$, doped in hydrochloric acid solution ($n_{HCl} = 10^{-5}$ mol/m^3). The measurements were carried out at $E_{pol,0} = 2 \times 10^5$ V × m^{-1}, T_{pol} = 300 K, c = 5.5 K/min.

Since there are no original experimental data on the activation energy U_0 and equilibrium concentrations of relaxers n_0 for muscovite crystals, for comparison with the theory, we determined them using three methods to calculate the parameter U_0: 1—initial ascent method (Garlica–Gibson); 2—Heat Velocity Variation Method (Bohuna–Buta); 3—the method based on the calculation of relaxation time [1,4]. The experimental equilibrium concentration of relaxers was calculated from an expression for the static dielectric permeability of thermo-stimulated depolarization $\varepsilon_0(\varepsilon_S - \varepsilon_\infty)E_{pol,0} = \frac{q_{ind}}{S} = \sigma_{ind}$, where ε_∞ represents the high-frequency dielectric permeability of the crystal. When accumulated (during polarization in stationary electric field) on flat capacitor plates, the charge $q_{ind} = \sigma_{ind}S$, is computed in an equal polarization time t_{pol}, and the surface density of the charge induced in dielectric $\sigma_{ind} = \int_0^{t_{pol}} j_{pol}(t)dt = P_{pol}\left(t_{pol}\right) \approx \frac{n_0 E_{pol,0} q^2 \delta_0^2}{12 k_B T_{pol}}$, computed by an approximate formula of the classical dipole polarization theory $P_{pol}\left(t_{pol}\right) \approx \frac{n_0 p_0^2 E_{pol,0}}{3 k_B T_{pol}}$ at $p_0 = \frac{1}{2} q\delta_0$, is the area below the curve corresponding to the individual experimental TSDC density maximum $\sigma_{ind} = \int_0^\infty j_{depol}(t)dt = \frac{1}{c}\int_{T_0}^\infty j_{depol}(T)dT$.

A comparison of TSDC spectra and activation energies implies that a maximum of 2, both crystalline sulfate and silicates, is caused by the relaxation of ion defects H_3O^+, and a maximum of 6 is due to the formation of complexes "vacancy + L-defect" (VL) or "vacancy + D-defect" (VD) [1]. In [1], the activation energy of complexes VL (VD) is estimated to be equal to 0.4–0.5 eV, which is comparable to the results (Tables 1–4). The formation of complexes of interstitial molecules with L- and D-defects [1] is not excluded. The types of relaxers and their orientation are indicated in Tables 1–4.

Ion OH^- activation energies calculated from the infrared and combination scattering spectra [1,4] and obtained for a maximum of 5 in the TSDC density spectra (Tables 1–4). These coincide with the error range, so a maximum of 5 is associated with ion OH^- relaxation. The low-temperature, first ordinal number in the TSDC density spectrum is strongly associated, as noted in Section 1 of this paper, with the tunneling of protons within and between anions.

The third and fourth maxima weaken in amplitude when HBC-class crystals are calcinated at temperatures of 373–473 K, wherein, when calcinated to temperatures 473–573 K disappears at the fourth maximum and, at 873–1373, K disappears at the third maximum, which allows for them to be connected with the movement of dipole molecules' crystallizing (structural) water and adsorbed water (on bundles) [1,4].

A comparison of the theoretical and experimental values of relaxer parameters in the natural phlogopite $KMg_3(AlSi_3O_{10})(OH)_2$ shows that, at temperatures of 178 K and 206 K (Figure 1 [1,4]), where structural defects associated with the relaxation of structural and adsorbed water molecules, respectively, are activated, the theoretical activation energy is 0.01 eV higher than the experimental one, and at temperatures of maxima 235 K (Figure 1) and 260, the theoretical values of activation energy fall within the confidence interval of measurements (Table 1).

At low temperatures, there is a significant discrepancy between the experiment and the results of calculations: at the temperature of 130 K (Figure 1) in the experiment, the ions H_3O^+ relaxes with an activation energy 0.17 ± 0.02 eV, and according to the calculation results $U_0 = 0.18$ eV, in the vicinity of the maximum associated with the tunneling transitions of protons between layers of water molecules and ions SiO_4^{4-}, the measured activation energy is equal to 0.05 ± 0.01 eV, and the calculated energy is 0.08 eV. In addition, in the vicinity of low-temperature maxima, the theoretical values of the equilibrium concentration are two orders of magnitude lower than the experimental ones [1,4].

For natural mineral onot talc $Mg_3(Si_4O_{10})(OH)_2$, the TSDC maxima were observed at temperatures of 86 K, 112 K, 180 K, 206 K, 230 K, 251 K, 305 K (Figure 2) [1,4].

According to Tables 1 and 2, a more rigorous account of proton tunneling brought the calculated values of activation energy closer to the measured values for low-temperature Bjerrum ionization defects H_3O^+, which are responsible for the monorelaxation maximum of the TSDC density at a temperature of 130 K (Table 1) in the natural phlo-

gopite $KMg_3(AlSi_3O_{10})(OH)_2$ and at the temperature of 112 K in onot talc (Table 2) $Mg_3(Si_4O_{10})(OH)_2$.

Phlogopite structure $KMg_3(AlSi_3O_{10})(OH)_2$ is characterized by the fact that the distance between the layers SiO_4^{4-} does not exceed 1.8 Å; that is, it is no more than the length of the hydrogen bridge [1]. Therefore, according to the calculation results (Table 1), we can assume two possibilities for the diffusion of defects in H_3O^+:

1. Ion migration H_3O^+ along the water layer and between H_2O molecules of neighboring layers;
2. Ion migration H_3O^+ between a layer of water molecules and a layer of ions SiO_4^{4-}.

In phlogopite crystals, two layers of anionic groups SiO_4^{4-}, associated with aluminum ions form two layers oriented perpendicular to the crystalline axis C. There are molecules in some of the potassium nests while, in some interpacket zones, there are continuous monomolecular water layers. Considering the dense packing of the layers, it is possible to allow for the electron shells of oxygen ions belonging to anions SiO_4^{4-} and neighboring water molecules to overlap. As a result, both the tunneling and over-barrier transitions of the proton from the H_3O^+ ion, formed in the water layer near the SiO_4^{4-} anion, are facilitated.

The results of the quantum mechanical calculation of the relaxer parameters (Tables 1 and 2) in the natural phlogopite $KMg_3(AlSi_3O_{10})(OH)_2$ and onot talc $Mg_3(Si_4O_{10})(OH)_2$ confirm the following Bjerrum defect migration scheme for H_3O^+:

Defect formation in H_3O^+ in the water layer or due to the introduction of proton–donor impurities is as follows:

$$H_2O + H^+ \rightarrow H_3O^+.$$

The transition from ion H_3O^+ to anion SO_4^{2-}, for the formation of a protonated $HSiO_4^{3-}$ anion, is as follows:

$$H_3O^+ + SiO_4^{4-} \rightarrow H_2O + HSiO_4^{3-}.$$

3. The reorientation of a protonated anion due to the transition of protons inside it:

$$HSiO_4^{3-} \rightarrow SiO_4H^{3-}.$$

4. The transition of a proton between cells of the anionic sublattice, where the newly formed protonated anion acquires the opposite orientation:

$$SiO_4H^{3-} \rightarrow HSiO_4^{3-}.$$

5. Reorientation of the second protonated anion:

$$HSiO_4^{3-} \rightarrow SiO_4H^{3-}.$$

6. The transition of a proton to a water molecule and the formation of a defect in H_3O^+:

$$SiO_4H^{3-} + H_2O \rightarrow SiO_4^{4-} + H_3O^+.$$

For natural muscovite $KAl_2(AlSi_3O_{10})(OH)_2$, TSDC maxima were observed at temperatures of 105 K, 153 K, 190 K, 206 K, 230 K, 246 K, 295 K (Figure 3) [1,4].

According to Table 3, the similarity of the chemical structure of muscovite to crystals of phlogopite and onot talc determines the commonality of the physical mechanism of the migration of ionization defects in H_3O^+, which are responsible for the monorelaxation maximum of the TSDC density at the temperature of 153 K (Table 3), associated with proton tunneling between layers of silicate anions SiO_4^{4-} and layers of water molecules.

Note that the experimental values of the energy activation of protons in the area of low-temperature maxima (in natural phlogopite: 0.05 ± 0.01 eV at 100 K; in onot talc: 0.06 ± 0.01 eV at 86 K; in muscovite: 0.04 ± 0.01 eV at 105 K) fall within the range of small values of this parameter for HBC (from 0.01 to 0.1 eV) [1]. At the same time, the theoretical

activation energy values computed for the data maxima by analytic Equation (27), taking into account the tunneling of protons, as is to be expected, are much closer to experimental values (computed by semi-empirical methods [1,4]) than those computed using only the thermal activation of protons on hydrogen bonds (Tables 1–3). Theoretical equilibrium concentrations of protons, calculated by tunneling, are also closer to the experimental ones (Tables 1–3). This circumstance makes it possible to reassert the commonality of the physical nature of data on thermally stimulated current maximums, connected in laminated silicates at temperatures T = 50–100 K, with the tunnel movement of protons inside and between silicate anions SiO_4^{4-} [1,2,69].

It is not difficult to see that the influence of tunneling on dielectric relaxation in laminated silicates also appears for the high-temperature (290–450 K) maximum of TSDC density associated with volumetric charge polarization (nonlinear bulk charge relaxation) caused by a relaxation movement of mixed type (due to the movement of structural defects H_3O^+, OH^-, H^+) [1]. Here, according to Tables 1–3, the experimental values of the energy activation of protons (in natural phlogopite: 0.35 ± 0.05 eV at 405 K; in onot talc: 0.40 ± 0.06 eV at 305 K; in muscovite: 0.38 ± 0.06 eV at 295 K) fall within a range of values from 0.3 to 0.45 eV. At the same time, the values of theoretical activation energies computed considering quantum effects, as well as at low temperatures, are closer to the experimental values than those computed with only classical proton transitions (Tables 1–3). The theoretical values of equilibrium concentrations computed for proton tunneling are also closer to experimental values than those computed for thermal activation only (Tables 1–3).

The experimental spectra of thermally stimulated depolarization current density for the chemically pure chalcanthite crystals $CuSO_4 \cdot 5H_2O$ were measured with the help of the empirical schemes developed and described in [68] and are presented (depicted) in Figure 4.

The experimental values of U_0, n_0 for chalcanthite crystals were calculated in this paper by famous quasi-empirical methods [1,4] and are shown in Table 4. The theoretical values of U_0, n_0 for chalcanthite were calculated based on Equation (22) with the MCF method [69], and are also presented in Table 4.

For chalcanthite crystals, on the basis of the Equation (22), similar results were obtained, and in the region of the low-temperature maximum of the TSDC density (94 K, Graph 1 in Figure 4), due to processes in protonated anions HSO_4^-, the theoretical activation energy ($U_0 = 0.16$ eV) is two times higher than the experimental one ($U_0 = 0.07 \pm 0.01$ eV, Table 4), which, taking into account the errors of the quasi-classical theory, falls within the confidence interval of the measured values.

According to the results of an X-ray analysis of the crystal structure $CuSO_4 \cdot 5H_2O$, two possibilities for the displacement of H_3O^+ defects [1] can be proposed:

1. Ion migration H_3O^+ along and between adjacent water layers;
2. Ion migration H_3O^+ between a layer of water and a layer of sulfate ions SO_4^{2-}.

Mixed motion is also possible along the layer—between interstitial water molecules and SO_4^{2-} ions.

The results of the quantum mechanical calculation of the relaxer parameters (Table 4) confirm the following Bjerrum defect migration scheme H_3O^+ (Figure 5):

1. Defect H_3O^+ formations are found in the water layer or due to the introduction of proton-donor impurities:
$$H_2O + H^+ \rightarrow H_3O^+.$$
2. A transition from H_3O^+ ion to SO_4^{2-} anion can form a protonated HSO_4^- anion:
$$H_3O^+ + SO_4^{2-} \rightarrow H_2O + HSO_4^-.$$
3. A protonated anion can be reoriented due to the transition of protons inside it:
$$HSO_4^- \rightarrow SO_4H^-.$$

4. If a proton undergoes a transition between cells of the anionic sublattice, the newly formed protonated anion acquires the opposite orientation:

$$SO_4H^- \rightarrow HSO_4^-.$$

5. Reorientation of the second protonated anion occurs:

$$HSO_4^- \rightarrow SO_4H^-.$$

6. The transition of a proton to a water molecule and formation of a defect in H_3O^+ can occur as follows:

$$SO_4H^- + H_2O \rightarrow SO_4^{2-} + H_3O^+.$$

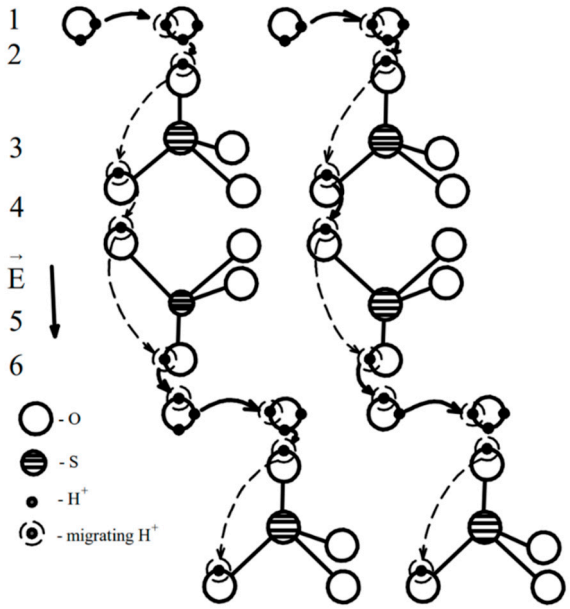

Figure 5. Scheme of H_3O^+ ion movement due to the gradual transfer of the proton in a chalcanthite crystal $CuSO_4 \cdot 5H_2O$. The arrows show the movement of the proton; the numbers indicate the stages of its movement.

A similar mechanism can be applied to study ion migration OH^-; however, in this case, the defect will move in the opposite direction. It should be noted that when the ions H_3O^+ and OH^- move along hydrogen bonds under the action of an electric field, their influence on the orientation of water molecules and anions SO_4^{2-} is the opposite.

The contribution of L and D defects and VL(VD) complexes to the electrical conductivity is possible, but very small (as mentioned above). The mechanism of their movement from layer to layer will differ at the initial stage of the formation of orientational defects, since the proton will approach the ion SO_4^{2-} only after the rotation of the water molecule. H_3O^+- conductivity at elevated temperatures could be considered proton conductivity; however, as the experiment showed, protons play only an intermediate role.

The Relaxer parameter numerical values (Table 4) obtained for chalcanthite (mineralogical characteristics of hydrated copper sulfates, along with other aqueous sulfates, such as epsomite $MgSO_4 \cdot 7H_2O$, melenterite $FeSO_4 \cdot 7H_2O$, morezonite $NiSO_4 \cdot 7H_2O$, gypsum $CaSO_4 \cdot 2H_2O$, etc.), as in the case of laminated silicates, indicate the dominant role of tunneling dielectric relaxation protons in the low-temperature area, since the maximum density of TSDC (measured at 94 K (graph 1 in Figure 4) with an activation energy of 0.07 ± 0.01 eV) is characterized. Taking into account the quantum effects, the theoretical calculated energy of activation is equal to 0.08 eV and, excluding tunneling, 0.16 eV. At high temperatures, in the field of non-linear volumetric charge polarization (290 K (graph 1 in Figure 4; Table 4)),

a comparison of the numerical values of activation energy calculated from the experiment (0.34 ± 0.04 eV) and phenomenological theory (based on Equation (24)), respectively, is presented, considering tunneling (0.35 eV) and thermal activation only (0.41 eV). This points to the significant influence of quantum kinetic phenomena on proton-relaxation polarization in crystalline hydrates.

The mechanism of migration of defects in H_3O^+ due to the gradual transfer of the proton described in Figure 5 can be used write the refined chemical formula of a chalcanthite crystal, from the perspective of the geometrical location of the main structural elements in the tetrahedral elementary cell of the complex compound $\left[Cu^{2+}\cdot 4H_2O\right]\cdot\left[{SO_4}^{2-}\right]\cdot H_2O$.

Due to the commonality of the chemical structure and the geometry of the crystalline structures, an H_3O^+ ion transfer mechanism is implemented in materials such as crystalline hydrates by analogous hydrogen ion migration schemes, according to the detailed ion formulas of the class:

$$FeSO_4\cdot 7H_2O = \left[Fe^{2+}\cdot 6H_2O\right]\cdot\left[{SO_4}^{2-}\right]\cdot H_2O,$$
$$MgSO_4\cdot 7H_2O = \left[Mg^{2+}\cdot 6H_2O\right]\cdot\left[{SO_4}^{2-}\right]\cdot H_2O,$$
$$NiSO_4\cdot 7H_2O = \left[Ni^{2+}\cdot 6H_2O\right]\cdot\left[{SO_4}^{2-}\right]\cdot H_2O.$$

The mineral moresonite $NiSO_4\cdot 7H_2O$ is characterized by emerald green or greenish white with glassy gloss, crystallized in an orthorombic system. It occurs as small crystals, stalactites or crusts. Natural crystals are needle-shaped, and synthetic–prismatic. Moresonite is soluble in water and dehydrates in open air, turning into $NiSO_4\cdot 6H_2O$ [70].

Magnesium sulfate, magnesium sulfate $MgSO_4$ (salt, colorless crystals, density 2.66 g/cm^3. At 1100–1200 °C, it decomposes into MgO, SO_2, and O_2) [71]. The solubility of $MgSO_4$ in water at 20 °C, 25.2% by mass$MgSO_4$ forms crystalline hydrates with 1, 2, 3, 4, 5, 6, 7, and 12 water molecules [71]. At room temperature, it crystallizes from aqueous solutions into epsomite $MgSO_4\cdot 7H_2O$ (Epsom salt). It is also found in nature as a mineral of kizerite $MgSO_4\cdot H_2O$. Alkaline salts with $MgSO_4$ form double salts, including naturally occurring langbeinite $K_2SO_4\cdot 2MgSO_4$, astrakhanite $Na_2SO_4\cdot MgSO_4\cdot 4H_2O$, polygalite $Na_2SO_4\cdot MgSO_4\cdot 2Ca_2SO_4\cdot 2H_2O$ and cainite $KCl\cdot MgSO_4\cdot 3H_2O$ [72,73].

We also note the appearance of aqueous sodium sulfate $Na_2SO_4\cdot 10H_2O$ mineral mirabilite (Glauber's salt) [72,73].

Regardless of whether there is an even or odd number of water molecules in the sulfate-based expression, the H_3O^+ ion transfer mechanism in the electric field remains similar to the one described above (Figure 5).

Let us return to the question of the theoretical spectra of thermally stimulated currents in the HBC. Equation (27), in conjunction with the MCF method, allows for the construction of the theoretical dependencies of TSDC density $j_{th}(T)$ in the vicinity of temperatures $T_{exp,max}$ of corresponding maxima 1–7 experimental graphs (graph 1 for phlogopite in Figure 1; graph 1 for onot talc in Figure 2; graph 4 for muscovite in Figure 3; graph 1 for chalcanthite in Figure 4). At the same time, theoretical graphs $j_{th}(T)$ were constructed by mathematical modeling (using the MathLab program) by a computer-assisted search on a set of theoretical numerical values for the parameters of relaxers $\varsigma_{0,th} = \{U_{0,th}; \delta_{0,th}; \nu_{0,th}; n_{0,th}; a_{th}\}$, provided that the difference between the calculated theoretical $T_{th,max} = \Psi\left(\varsigma_{0,th}; j_{th,max}\right)$ and experimental temperature $T_{exp,max} = \Phi\left(\varsigma_{0,exp}; j_{exp,max}\right)$ of each measured maximum density of TSDC is minimized. At the same time, the theoretical calculation of the amplitude of the current density of the thermally stimulated depolarization $j_{th,max} = j_{th}\left(\varsigma_{0,th}; T_{th,max}\right)$, calculated from analytical expressions, can differ significantly from the measured values $j_{exp,max} = j_{exp}\left(\varsigma_{0,exp};\ T_{exp,max}\right)$.

In general, Equation (22), studied by the MCF method of the set of parameters $\varsigma_{0,th}$ from a comparison with experimental data $\varsigma_{0,exp}$ in the surrounding area (on the set of measures of the continuum) of each point $\left(T_{exp,max}; j_{exp,max}\right)$ of TSDC density, which

provides a set of theoretical graphs $j_{th}(T)$ of curves, each tied to its experimental point and its surroundings. In essence, graph $j_{th,i}(T)$, computed for a single i-th experimental maximum, corresponds to the decomposition of a generalized (theoretically not yet studied) function $j_{th,whole}(T)$ into a power series by parameter $\frac{T-T_{exp,max}}{T_{exp,max}}$, while retaining the number of series members corresponding to the degree of precision of the mathematical model. The rigorous study of function $j_{th,whole}(T)$ over the entire temperature range of the experimental spectrum $j_{exp,whole}(T)$ is the subject of a separate study.

To calculate a separate theoretical graph $j_{th}(T)$, we apply Equation (22), in which the relaxation time $\tau_{depol}(T) = \frac{1}{2\Omega_{depol}(T)}$ is calculated in a temperature function based on the absence of an electric field:

$$\Omega_{depol}(T) = \frac{\nu_0}{2} \times \frac{\exp(-\Lambda) - \frac{\Lambda}{X}\exp(-X)}{1 - \frac{\Lambda}{X}}. \quad (23)$$

Transformations are established in Equation (22) considering the Equation (23), according to $X = \frac{U_0}{k_B T}$, $\Lambda = \frac{\pi\delta_0\sqrt{mU_0}}{\hbar\sqrt{2}}$, based on

$$B(T) = \frac{1}{c}\int_{T_0}^{T} \frac{dT}{\tau_{depol}(T)} = -\frac{U_0}{ck_B}\int_{X_0}^{X} \Omega_{depol,0}(X) \times \frac{dX}{X^2} = \frac{\nu_0 U_0}{ck_B\Lambda}\int_{\frac{\Lambda}{X_0}}^{\frac{\Lambda}{X}} \frac{\exp(-\Lambda) - u\exp\left(-\frac{\Lambda}{u}\right)}{1-u} \times du,$$

applying notation $b = \frac{\nu_0 U_0}{ck_B\Lambda}$, we have

$$B(T) = b\left(\exp(-\Lambda) \times ln\left(\frac{1-\frac{\Lambda}{X_0}}{1-\frac{\Lambda}{X}}\right) - A(T)\right).$$

Here,

$$A(T) = \int_{\frac{\Lambda}{X_0}}^{\frac{\Lambda}{X}} \frac{u\exp\left(-\frac{\Lambda}{u}\right)}{1-u} \times du.$$

This integral, which reflects the specific effect of temperature on the thermally stimulated depolarization current, is studied by numerical methods [68].

Denote $j_{depol,0} = q\delta_0 \times \Delta n_{pol}$.

Then, Equation (22) takes a convenient form for numerical analysis

$$j_{th}(T) = j_{depol}(T) = j_{depol,0} \times \Omega_{depol}(T) \times \exp(-B(T)). \quad (24)$$

In Equation (24), expressions $\Omega_{depol}(T)$, $B(T)$ are monotonically increasing functions of temperature.

In expression $j_{depol,0}$, function $\Delta n_{pol} = \frac{1}{3}n_0 \times \frac{\Xi_{st,pol}}{2\Omega_{st,pol}}$ is computed at the polarization temperature T_{pol} and intensitypolarizing field $E_{pol,0}$, with the help of Equations (18) and (19). Nonlinear dependencies are as follows:

$$\Omega_{st,pol} = \frac{\nu_0}{2}\left(\exp\left(-X_{pol}\right)ch\left(\xi_{0,pol}\right) + \frac{\frac{1}{2}\exp(-\Lambda)\exp\left(\eta_{0,pol}\right)\left(1+\exp\left(-2\xi_{0,pol}\right)\right) - \exp\left(-X_{pol}\right)ch\left(\xi_{0,pol}\right)}{1-\frac{\Lambda}{X_{pol}}}\right), \quad (25)$$

$$\Xi_{st,pol} = \nu_0\left(\exp\left(-X_{pol}\right)sh\left(\xi_{0,pol}\right) + \frac{\frac{1}{2}\exp(-\Lambda)\exp\left(\eta_{0,pol}\right)\left(1-\exp\left(-2\xi_{0,pol}\right)\right) - \exp\left(-X_{pol}\right)sh\left(\xi_{0,pol}\right)}{1-\frac{\Lambda}{X_{pol}}}\right). \quad (26)$$

Here, $\xi_{0,pol} = \left|\frac{(\Delta U)_{0,pol}}{k_B T_{pol}}\right|$, $\eta_{0,pol} = \Lambda\left|\frac{(\Delta U)_{0,pol}}{U_0}\right|$, $(\Delta U)_0 = \frac{1}{6} q \delta_0 (\varepsilon_\infty + 2) E_{0,pol}$.

Figures 6–9 show theoretical graphs $j_{th}(T)$, calculated according to the described methodology by Equation (24) against the background of the measured spectra of density TSDC in crystals of natural phlogopite, onot talc, muscovite, and chalcanthite.

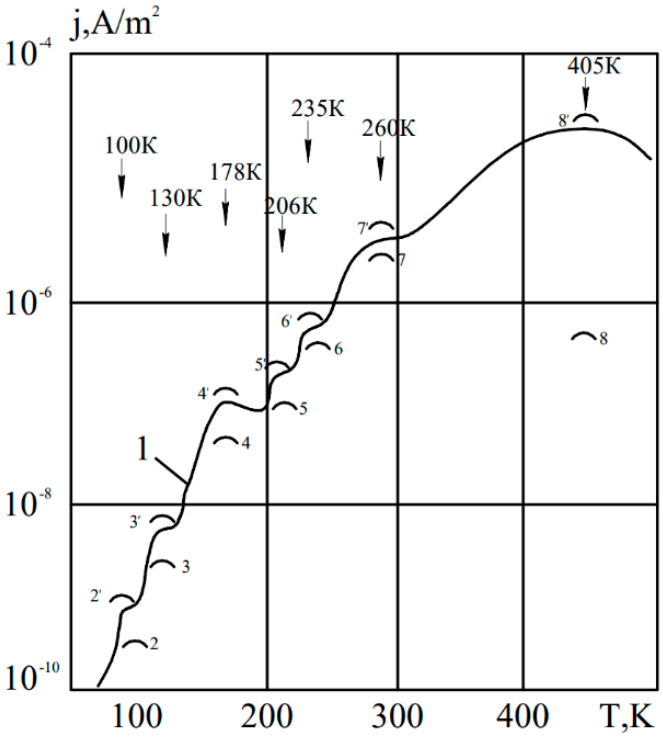

Figure 6. Graphs of TSDC density in natural phlogopite: 1—experimental spectrum (graph 1 in Figure 1); 2–8, 2′–8′—theoretical charts $j_{th}(T)$.

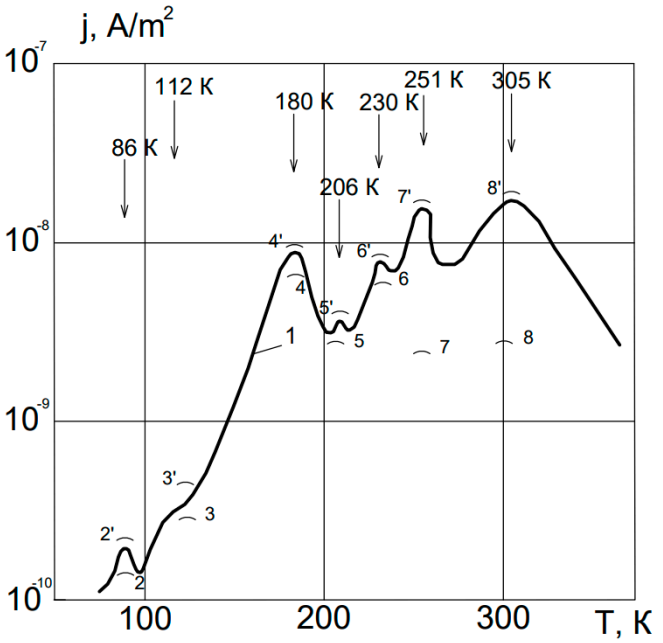

Figure 7. Graphs of TSDC density in onot talc: 1—experimental spectrum (graph 1 in Figure 2); 2–8, 2′–8′—theoretical charts $j_{th}(T)$.

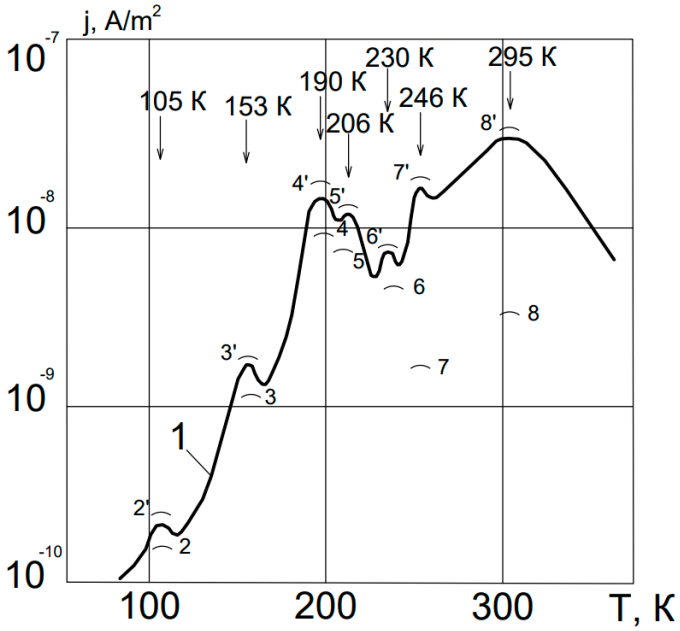

Figure 8. Graphs of TSDC density in muscovite: 1—experimental spectrum (graph 4 in Figure 3); 2–8, 2′–8′—theoretical charts $j_{th}(T)$.

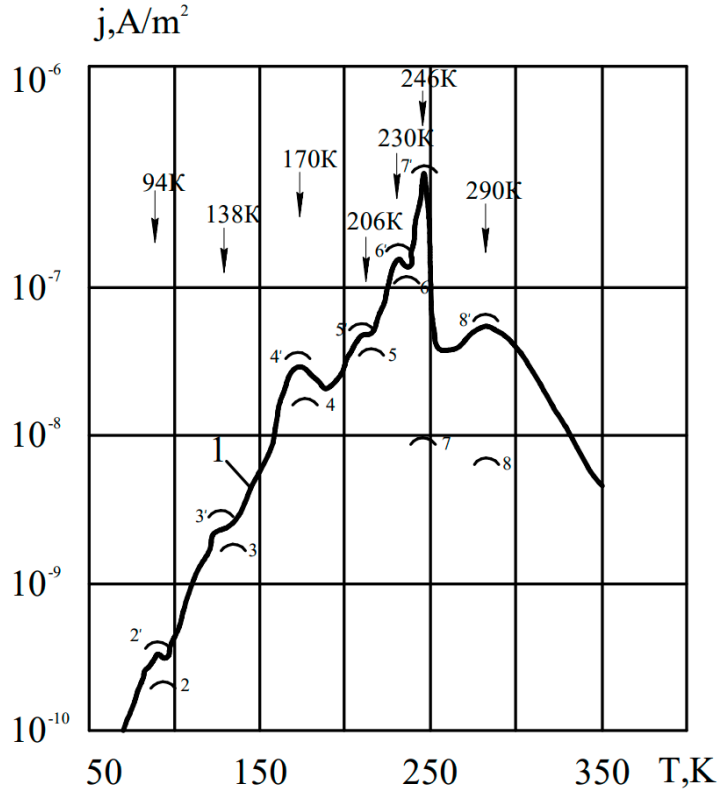

Figure 9. Graphs of TSDC density in chemically pure chalcanthite: 1—experimental spectrum (graph 1 in Figure 4); 2–8, 2′–8′—theoretical charts $j_{th}(T)$.

In Figures 6–9: 2–8, the theoretical graphs are calculated, taking into account only the thermal activation of protons within the classical model of dipole polarization [1,3] when Equation (24) is simplified

$$j_{th,class.}(T) = j_{depol,class.}(T) = P_{pol}\left(t_{pol}\right) \times \Omega_{depol,class.}(T) \times \exp(-B_{class.}(T)). \quad (27)$$

Here,

$$P_{pol}\left(t_{pol}\right) \approx \frac{n_0 E_{pol,0} q^2 \delta_0^2}{12 k_B T_{pol}}, \Omega_{depol,class.}(T) = \frac{\nu_0}{2} \times \exp(-X) = \frac{\nu_0}{2} \times \exp\left(-\frac{U_0}{k_B T}\right),$$

$$B_{class.}(T) = \frac{1}{c} \int_{T_0}^{T} \frac{dT}{\tau_{depol,class.}(T)} = -\frac{\nu_0 U_0}{c k_B} \int_{\frac{\Lambda}{X_0}}^{\frac{\Lambda}{X}} \exp(-X) \times \frac{dX}{X^2} = \frac{\nu_0 U_0}{c k_B \Lambda} \int_{\frac{\Lambda}{X_0}}^{\frac{\Lambda}{X}} \exp\left(-\frac{\Lambda}{u}\right) \times du.$$

In Figures 6–9: 2′-8′, show the theoretical graphs calculated by Equation (27), taking into account the thermal activation and tunneling of protons, and the temperature values $T_{exp,max}$ of the respective maxima 1–7 of the experimental spectrum $j_{exp,whole}(T)$.

In Figures 6–9, the number of theoretical graphs is greater by 1 compared to the corresponding experimental maximums.

4. Discussion

From the analysis of the graphs in Figures 6–9, it is clear that theoretical curves 3′-6′(computed by a stricter theory, taking into account the tunneling of protons) are situated slightly higher and closer, and theoretical curves 3–6 (calculated according to the classical model of dipole polarization, taking into account only the thermal activation of protons) are located lower and a little further along the amplitude of the current density relative to the corresponding experimental maximums 2–6. In fact, this situation is quite qualitative and reflects both methods (both classical and quantum) regarding the description of properties and theoretical spectra parameters of density TSDC in HBC in the temperature range T = 100–235 K, where polarization is dipole and is related to the relaxation movement of Bjerrum orientation defects and the rotation of water molecules in the electric field.

The theoretical curves 2′ are markedly closer and curve 2 is noticeably further along the amplitude to the experimental maximum 1. Thus, considering the effects of proton tunneling on low-temperature polarization (50–100 K), the results of or the model of a double-symmetric potential pit (not considering the influence of electric field irregularities in the matter) show a marked convergence with the results of the theory and experiment (the same can be seen in Tables 1–4).

The theoretical curves 7, 8 (calculated according to the classical linear model of dipole polarization, taking into account only the thermal activation of protons) are situated significantly lower (by three to four orders) by amplitude to the experimental maxima 6, 7. At the same time, considering the effects of proton tunneling on the nonlinear polarization model at the theoretical level, according to the curves 7′, 8′, provides an almost complete consistency with the results of the theory and experiment on the amplitude density TSDC in HBC.

Thus, taking into account the effects of proton tunneling against the background of the nonlinear dependences embedded in Equation (24) on the dimensionless polarization parameters $\xi_{0,pol}$, $\eta_{0,pol}$ leads to a more rigorous effect, in comparison with the classical linear theory according to Equation (27), of the polarizing field strength $E_{pol,0}$ on polarization at high temperatures (230–550 K). First of all, this effect refers to the volume–charge polarization (290–450 K), the formation of which, in the HBC, proceeds with a significant dependence on quantum effects (the same can be seen in Tables 1–4).

The results obtained in this paper are relevant and scientifically significant for a number of areas of modern science, particularly for the development of theoretical ideas about the quantum mechanisms of the formation of the ferroelectric state due to the tunnel motion of protons in the hydrogen sublattice of KDP, DKDP crystals, which are of significant practical importance for laser technology (regulators of radiation parameters), nonlinear optics and optoelectronics (electro-optical sensors, strain sensors of hard rocks and building materials, machine parts and mechanisms, etc.) [45–54], and information technology (thin-film ferroelectric elements of microcircuits for high-speed, non-volatile storage devices with an abnormally long time maintaining the residual polarization (up to 10 years)) [29–44].

5. Conclusions

This work is devoted to improving the schemes and methods of the existing quasi-classical kinetic theory of dielectric relaxation [1–5] and, on this basis, numerical calculations of the parameters of relaxers (protons) in HBC over a wide temperature range (50–550 K) and fields (0.1–1 MV/m). The subject of these improvements is the development of a more stringent, in comparison with [1–5], theoretical method to consider the effects of corrections to the non-stationary quantum transparency of a parabolic potential barrier caused by an electric field. In previous works [1,6], such corrections to the parabolic potential barrier were not calculated. A double-symmetrical potential pit with a parabolic potential barrier was adopted as a geometric model of the crystalline potential field. The solutions of the nonlinear quasi-classical kinetic Equation (11), in continuation [1,6], are constructed in the most general form in Equation (16), considering the additional elements of $\exp(-2\xi(t))$ in expressions for non-stationary quantum transparency in Equations (7) and (8). The diffusion and mobility coefficients of protons are constructed to model the parabolic double-symmetric potential well of forms that are perturbed by an external variable field in Equations (9) and (10).

The Bucci–Rive phenomenological formula (Equation (22)) for thermally stimulated depolarization current density (TSDC) was first written first, considering the stationary quantum transparency of the parabolic potential proton barrier (Equation (24)). When calculating the initial polarization of the crystal, the updated stationary Equations (17)–(19) obtained in this work were used. Previously, these tasks were not solved. In this case, the choice of the parabolic form of the potential barrier allows, at the theoretical level, for the mathematical model to be brought closer to the real spatial structure of the crystalline potential field. This is evident from the comparison of the numerical values of the relaxer parameters (activation energy, equilibrium concentration) calculated from the experiment and on the basis of Equation (22), considering tunneling and excluding proton tunneling, using the example of crystals of phlogopite, onot talc, muscovite and chemically pure chalcanthite (Tables 1–4). It can be seen from Tables 1–4 that accounting for proton tunnel transitions in the Equation (22) significantly approximates the theoretical values of activation energy and equilibrium concentration of protons relaxing in low-temperature (50–100 K) and in high-temperature (350–550 K) maxima regions of TSDC density, compared to their experimental values in HBC. Thus, in this work, at a higher theoretical level, in comparison with [4], it was confirmed that the quantum effects associated with proton tunnel transitions in the HBC anion sublattice dominate the region of low-temperature (50–100 K) TSDC maxima. In continuation of this [1,7], we found that quantum effects continue to significantly affect the dielectric relaxation kinetics in proton semiconductors and dielectrics (PSD) in the region of high-temperature (250–550 K) TSDC maxima.

At the same time, in continuation of [1,4], we carried out precision measurements of temperature spectra of TSDC density for chalcanthite crystals. The effect of alloying impurities' concentrations and crystal calcination temperatures on the properties and parameters of experimental maxima in the TSDC spectrum of chalcanthite was established.

We described, in the form of chemical equations, the physical mechanism of the quantum tunnel motion of HBC protons with a complex crystal structure (Figure 5).

A significant effect of proton tunneling on the amplitudes of theoretical TSDC density maxima has been established. It follows from Figures 6–9 that, taking into account quantum effects in the Bucci–Rive formula (Equation (24)), the theoretical amplitudes of TSDC can be approximated in comparison to experimental ones over almost the entire temperature range (50–550 K).

The above patterns indicate a fairly high degree of applied scientific significance for the theoretical results obtained in this article for the further development of physics and proton semiconductors and dielectrics (PSD) technology.

6. Patents

Kalytka V.A., Baimukhanov Z.K., Bashirov A.V., Khanov T.A., Isaev V.L. Suleimanov S.R. Patent of the Republic of Kazakhstan for utility model. Universal setup for measuring the parameters of microscopic structural defects. No.5016. 6 May 2020.

Author Contributions: Conceptualization, V.K.; methodology, V.K.; analytical and numerical calculations, V.K. and Z.B.; experimental studies, measurements, processing of experimental results, Z.B., A.M., P.D., O.G. and Y.N.; software, Y.N.; validation, V.K., Z.B. and Y.N.; formal analysis, V.K. and Y.S.; investigation, V.K., Z.B. and Y.N.; resources, V.K., Y.N., Z.B. and Y.S.; data curation, V.K., Y.S. and Y.N.; writing—original draft preparation, V.K.; project administration, Y.S. All authors have read and agreed to the published version of the manuscript.

Funding: This research received no external funding.

Institutional Review Board Statement: Not applicable.

Informed Consent Statement: Not applicable.

Data Availability Statement: Not applicable.

Conflicts of Interest: The authors declare no conflict of interest.

References

1. Kalytka, V.A. *Electrophysics of Proton Semiconductors and Dielectrics*; Karaganda Technical University, KTUPubl. House: Karaganda, Kazakhstan, 2021; 133p, ISBN 978-601-320-399-7.
2. Kalytka, V.; Bulatbayev, F.; Neshina, Y.; Bilichenko, Y.; Bilichenko, A.; Bashirov, A.; Sidorina, Y.; Naboko, Y.; Malikov, N.; Senina, Y. Theoretical Studies of Nonlinear Relaxation Electrophysical Phenomena in Dielectrics with Ionic–Molecular Chemical Bonds in a Wide Range of Fields and Temperatures. *Appl. Sci.* **2022**, *12*, 6555. [CrossRef]
3. Kalytka, V.A.; Mekhtiev, A.D.; Bashirov, A.; Yurchenko, A.V.; Al'Kina, A.D. Nonlinear Electrophysical PhenomenainIonic Dielectrics with a Complicated Crystal Structure. *Russ. Phys. J.* **2020**, *63*, 282–289. [CrossRef]
4. Tonkonogov, M.P. Dielectric spectroscopy of hydrogen-bonded crystals, and proton relaxation. *UspekhiFiz. Nauk.* **1998**, *41*, 25–48. [CrossRef]
5. Kalytka, V.A.; Korovkin, M.V. Quantum Effects at a Proton Relaxation at Low Temperatures. *Russ. Phys. J.* **2016**, *59*, 994–1001. [CrossRef]
6. Kalytka, V.A.; Korovkin, M.V. Dispersion Relations for Proton Relaxation in Solid Dielectrics. *Russ. Phys. J.* **2017**, *59*, 2151–2161. [CrossRef]
7. Kalytka, V.; Bashirov, A.; Taranov, A.V.; Tatkeyeva, G.G.; Neshina, Y.G.; Sidorina, Y.A. Methods of Theoretical Researches the Properties of Electrotechnical Materials Class of Dielectrics with Hydrogen Bonds. *J. Comput. Theor. Nanosci.* **2019**, *16*, 2799–2804. [CrossRef]
8. Kalytka, V.A.; Bashirov, A.V.; Tatkeyeva, G.G.; Sidorina, Y.A.; Ospanov, B.S.; Ten, T.L. The impact of the nonlinear effects on thermally stimulated depolarization currents in ion dielectrics. *Period. Eng. Nat. Sci.* **2021**, *9*, 195–217. [CrossRef]
9. Abrikosov, A.A. Resonance tunneling in high-temperature superconductors. *UspekhiFiz. Nauk.* **1998**, *168*, 683–695. [CrossRef]
10. Chang, L.; Esaki, L.; Tsu, R. Resonant tunneling in semiconductors double barrier. *Appl. Phys. Lett.* **1974**, *24*, 593–595. [CrossRef]
11. Grodecka, A.; Machnikowski, P.; Förstner, J. Phonon-assisted tunneling between singlet states in two-electron quantum dot molecules. *Phys. Rev. B* **2008**, *78*, 085302. [CrossRef]
12. Imry, Y.; Tinkham, M. Introduction to Mesoscopic Physics. *Phys. Today* **1998**, *51*, 60. [CrossRef]
13. Iogansen, L.V. On the possibility of resonant transfer of electrons in crystals through the barrier system. *ZhETF* **1963**, *45*, 207–218.
14. Iogansen, L. Thin-film electron interferometers. *UspekhiFiz. Nauk.* **1965**, *86*, 175–179. [CrossRef]
15. Mattia, J.P.; McWhorter, A.L.; Aggarwal, R.J.; Rana, F.; Brown, E.R.; Maki, P. Comparison of a rate-equation model with experiment for the resonant tunneling diode in scattering-dominated regime. *J. Appl. Phys. Lett.* **1998**, *84*, 1140–1148. [CrossRef]
16. Tryukhan, T.A.; Stukova, E.V.; Baryshnikov, S.V. Dielectric properties triglitsinsulfat in porous matrices. *Acad. J. Izv. Samara Sci. Cent. Russ. Acad. Sci. Ser. Phys. Electronic.* **2010**, *12*, 4.
17. Stankowska, J.; Czosnowska, E. Effect of grown conditions on the domain structure of triglycine sulphate crystals. *Acta Phys. Polon.* **1975**, *A43*, 641–644.
18. Yacenko, O.B.; Chudotvortsev, I.G.; Stekhanova, G.D.; Milovidova, S.D.; Hogasinskaya, O.V. Density and contents of water in tryglycinsulfate crystals. *Bull. Voronezh State Univ. (VGU) Ser. Chem. Biol. Pharm.* **2006**, *2*, 117–121.
19. Tsedrik, M.S. *Physical Properties of Triglycine Sulfate Crystals (Depending on Growing Conditions)*; Science and Technology: Minsk, Belarus, 1986; 216p.
20. Stekhanova, Z.D.; Yatsenko, O.B.; Milovidova, S.D.; Sidorkin, A.S.; Rogazinskaya, O.V.; Yuryev, A.N. Dielectric properties of crystals triglycine sulfate, grown from aqueous solutions at the temperatures below 0 °C. *Bull. Voronezh State Univ. (VGU) Ser. Chem. Biol. Pharm.* **2004**, *2*, 46–49.

21. Yatsenko, O.B. Effect of temperature and water content on the properties of triglycine sulfate crystals. In Proceedings of the Fourth International Symposium "Fractals and Applied Synergetics", Moscow, Russia, September 2005; pp. 1–181.
22. Stekhanova, Z.D. Properties of triglycine sulfate crystals grown from aqueous solutions. *Russ. J. Appl. Chemist.* **2005**, *78*, 45–51. [CrossRef]
23. Strukov, B.A.; Yakushkin, E.D. Local sound velocity and growth defectsin triglycine sulfate crystals. *IT* **1978**, *20*, 1538–1540.
24. Prasolov, B.N.; SafonovaI, A. Influence of the rate and direction of passage of a second-order phase transition on dielectric losses in tgs crystals. *Proc. Acad. Sci. USSR Ser. Phys.* **1993**, *57*, 47–49.
25. Rogazinskaya, O.V.; Milovidova, S.D.; Sidorkin, A.S.; Chernyshev, V.V.; Babicheva, N.G. Properties of nanoporous alumina with inclusions of triglycine sulfate and rochellesalt. *Phys. Solid State* **2009**, *51*, 1430. [CrossRef]
26. Ezhilvalavan, S.; Tseng, T.-Y. Progress in the developments of (BST) thin films for Gigabitera DRAMs. *Mater. Chem. Phys.* **2000**, *65*, 227–248. [CrossRef]
27. Kotecki, D.E.; Baniecki, J.D.; Shen, H.; Laibowitz, R.B.; Saenger, K.L.; Lian, J.J.; Shaw, T.M.; Athavale, S.D.; Cabral, C.; Duncombe, P.R.; et al. (Ba,Sr)TiO_3 dielectrics for future stacked-capacitor DRAM. *IBM J. Res. Develop.* **1999**, *43*, 367–382. [CrossRef]
28. Abdullaev, D.A.; Milovanov, R.A.; Volkov, R.L.; Borgardt, N.I.; Lantsev, A.N.; Vorotilov, K.A.; Sigov, A.S. Ferroelectric memory: State-of-the-art manufacturing and research. *Russ. Technol. J.* **2020**, *8*, 44–67. [CrossRef]
29. Izyumskaya, N.; Alivov, Y.; Morkoç, H. Oxides, oxides, and more oxides: High-κ oxides, ferroelectrics, ferromagnetics, and multiferroics. *Crit. Rev. Solid State Mater. Sci.* **2009**, *34*, 89–179. [CrossRef]
30. Izyumskaya, N.; Alivov, Y.-I.; Cho, S.-J.; Morkoç, H.; Lee, H.; Kang, Y.-S. Processing, Structure, Properties, and Applications of PZT Thin Films. *Crit. Rev. Solid State Mater. Sci.* **2007**, *32*, 111–202. [CrossRef]
31. Setter, N.; Damjanovic, D.; Eng, L.; Fox, G.; Gevorgian, S.; Hong, S.; Kingon, A.; Kohlstedt, H.; Park, N.Y.; Stephenson, G.B.; et al. Ferroelectric thin films: Review of materials, properties, and applications. *J. Appl. Phys.* **2006**, *100*, 051606. [CrossRef]
32. Eom, C.B.; Trolier-McKinstry, S. Thin-film piezoelectric MEMS. *MRS Bull.* **2012**, *37*, 1007–1021. [CrossRef]
33. Panda, P.K.; Sahoo, B. PZT to Lead Free Piezo Ceramics: A Review. *Ferroelectrics* **2015**, *474*, 128–143. [CrossRef]
34. Wouters, D.J.; Maes, D.; Goux, L.; Lisoni, J.G.; Paraschiv, V.; Johnson, J.A.; Schwitters, M.; Everaert, J.-L.; Boullart, W.; Schaekers, M.; et al. Integration of $SrBi_2Ta_2O_9$ thin films for high density ferroelectric random access memory. *J. Appl. Phys.* **2006**, *100*, 051603. [CrossRef]
35. Polakowski, P.; Müller, J. Ferroelectricity in undoped hafnium oxide. *Appl. Phys. Lett.* **2015**, *106*, 232905. [CrossRef]
36. Mueller, S.; Mueller, J.; Singh, A.; Riedel, S.; Sundqvist, J.; Schroeder, U.; Mikolajick, T. Incipient ferroelectricity in Al-doped HfO_2 thin films. *Adv. Functional. Mater.* **2012**, *22*, 2412–2417. [CrossRef]
37. Chernikova, A.G.; Kuzmichev, D.S.; Negrov, D.V.; Kozodaev, M.G.; Polyakov, S.N.; Markeev, A.M. Ferroelectric properties of full plasma-enhanced ALD TiN/La: HfO_2/TiN stacks. *Appl. Phys. Lett.* **2016**, *108*, 242905. [CrossRef]
38. Müller, J.; Böscke, T.S.; Bräuhaus, D.; Schröder, U.; Böttger, U.; Sundqvist, J.; Kücher, P.; Mikolajick, T.; Frey, L. Ferroelectric $Zr_{0.5}Hf_{0.5}O_2$ thin films for nonvolatile memory applications. *Appl. Phys. Lett.* **2011**, *99*, 112901. [CrossRef]
39. Starschich, S.; Schenk, T.; Schroeder, U.; Boettger, U. Ferroelectric and piezoelectric properties of $Hf_{1-x}Zr_xO_2$ and pure ZrO_2 films. *Appl. Phys. Lett.* **2017**, *110*, 182905. [CrossRef]
40. Sang, X.; Grimley, E.D.; Schenk, T.; Schroeder, U.; LeBeau, J.M. On the structural origins of ferroelectricity in H_fO_2 thin films. *Appl. Phys. Lett.* **2015**, *106*, 162905. [CrossRef]
41. Müller, J.; Polakowski, P.; Mueller, S.; Mikolajick, T. Ferroelectric hafnium oxide based materials and devices: Assessment of current status and future prospects. *J. Solid State Sci. Technol.* **2015**, *4*, N30–N35. [CrossRef]
42. Muller, J.; Boscke, T.S.; Muller, S.; Yurchuk, E.; Polakowski, P.; Paul, J.; Martin, D.; Schenk, T.; Khullar, K.; Kersch, A.; et al. Ferroelectric hafnium oxide: A CMOS-compatible and highly scalable approach to future ferroelectric memories. In Proceedings of the 2013 IEEE International Electron Devices Meeting, Washington, DC, USA, 9–11 December 2013. [CrossRef]
43. Schroeder, U.; Yurchuk, E.; Müller, J.; Martin, D.; Schenk, T.; Polakowski, P.; Adelmann, C.; Popovici, M.I.; Kalinin, S.V.; Mikolajick, T. Impact of different dopants on the switching properties of ferroelectric hafniumoxide. *J. Appl. Phys.* **2014**, *53*, 08LE02. [CrossRef]
44. Bystrov, V.S.; Paramonova, E.V.; Meng, X.; Shen, H.; Wang, J.; Fridkin, V.M. Polarization switching in nanoscale ferroelectric composites containing PVDF polymer film and graphene layers. *Ferroelectrics* **2022**, *590*, 27–40. [CrossRef]
45. Ronald, E. Cohen. Surface effects in ferroelectrics: Periodic slab computations. *Ferroelectrics* **1997**, *194*, 323–342. Available online: https://www.tandfonline.com/doi/abs/10.1080/00150199708016102 (accessed on 7 May 2011).
46. Belonenko, M.B. Characteristic features of nonlinear dynamics of a laser pulse in a photorefractive ferroelectric with hydrogen bonds. *Quantum Electron.* **1998**, *28*, 247–250. [CrossRef]
47. Strukov, B.A.; Levanyuk, A.P. *Ferroelectric Phenomena in Crystals. Physical Foundations*; Springer: Berlin/Heidelberg, Germany, 1998; 308p. [CrossRef]
48. Fridkin, V.M. Critical size in ferroelectric nanostructures. *Phys. Usp.* **2006**, *49*, 193–202. [CrossRef]
49. Levin, A.A.; Dolin, S.P.; Zaitsev, A.R. Charge distribution, polarization and properties of ferroelectrics of type KDP. *Chem. Phys.* **1996**, *15*, 1195–1204.
50. Kulagin,I A, Components of the third-order nonlinear susceptibility tensors in KDP, DKDP and $LiNbO_3$ nonlinear optical crystals. *Quantum Electron.* **2004**, *34*, 657. [CrossRef]
51. Okatan, M.; Mantese, J.; Alpay, S. Effect of space charge on the polarization hysteresis characteristics of monolithic and compositionally graded ferroelectrics. *Acta Mater.* **2010**, *58*, 39–48. [CrossRef]

52. Kayumov, D.; Bulatbaev, F.; Kayumova, I.; Breido, J.; Bulatbayeva, Y. An engineering approach for the qualitative assessment of the luminous flux of led lamps. *Int. J. Energy Clean Environ.* **2023**, *24*, 31–43. [CrossRef]
53. Mekhtiyev, A.D.; Bulatbayev, F.N.; Taranov, A.V.; Bashirov, A.V.; Neshina, Y.G.; Alkina, A.D. Use of reinforcing elements to improve fatigue strength of steel structures of mine hoisting machines (MHM). *Metalurgija* **2020**, *59*, 121–124.
54. Yurchenko, A.V.; Mekhtiyev, A.D.; Bulatbaev, F.N.; Neshina, Y.G.; Alkina, A.D.; Madi, P.S. Investigation of additional losses in optical fibers under mechanical action. *IOP Conf. Ser. Mater. Sci. Eng.* **2019**, *516*, 012004. [CrossRef]
55. Skinner, S.J. Recent advances in Perovskite-type materials for solid oxide fuel cell cathodes. *Int. J. Inorg. Mater.* **2001**, *3*, 113–121. [CrossRef]
56. Yaroslavtsev, A.B. Solid electrolytes: Main prospects of research and development. *Russ. Chem. Rev.* **2016**, *85*, 1255–1276. [CrossRef]
57. Yaroslavtsev, A.B. Proton conductivity of inorganic hydrates. *Russ. Chem. Rev.* **1994**, *63*, 429–435. [CrossRef]
58. Glöckner, R.; Neiman, A.; Larring, Y.; Norby, T. Protons in $Sr_3(Sr_{1+x}Nb_{2-x})O_{9-1.5x}$ perovskite. *Solid State Ion.* **1999**, *125*, 369–376. [CrossRef]
59. Animica, I.E. High temperature proton conductors with structural disordering of the oxygen sublattice. *Russ. J. Electrochem.* **2009**, *45*, 712–721.
60. Capasso, F.; Sen, S.; Beltram, F.; Cho, A.Y. Resonant Tunnelling and Superlattice Devices: Physics and Circuits. In *Physics of Quantum Electron Devices*; Springer Series in Electronics and Photonics; Springer: Berlin/Heidelberg, German, 1990; Volume 28, pp. 181–252. [CrossRef]
61. Khusnullina, A.L.; Voskoboynikova, O.B. Automated System of Collection and Visualization of Technological Data in Production of Semiconductor Devices. *Vestn. NSU. Ser. Inf. Technol.* **2017**, *15*, 100–110. [CrossRef]
62. Krotov, K.V. Gradient Method of Creating the Dynamic Scheduling of Processing Data in a Conveyor System at Different Points in Time of Their Receipt. *Bull. NSU. Ser. Inf. Technol.* **2016**, *14*, 39–60.
63. Timokhin, V.M. Multifunctional Device for Studying the Physical and Technical Characteristics of Semiconductors, Dielectrics and Electrically Insulating Materials. Patent for the Invention Russian Federation Bulletin No. 6, 27 February 2009.
64. Tikhomirov, P.O.; Emelyanov, P.V.; Plotnik, N.S.; Zyryanov, A.V. Minimizing downtime processes during their migration in the cloud. *Bull. NSU. Ser. Inf. Technol.* **2014**, *12*, 112–120.
65. Ivanov, V.N. Numerical methods of studying mechanical systems with additional connections. *Bull. Ofperm Univ. Ser. Math. Mech. Comput. Sci.* **2015**, *31*, 16–27.
66. Solodushkin, A.I.; Kibitkin, V.V.; Pleshanov, V.S. A modified algorithm for calculating the field of displacement vectors for assessing deformation. *Izv. Tomsk. Polytech. Univ. Ser. Manag. Comput. Comput. Sci.* **2011**, *318*, 48–51.
67. Kalytka, V.A. Investigating the scheme of numerical calculation the parameters of non-linear electrophysical processes by minimizing comparison function method. Space, time and fundamental interactions. *Publ. House PROFIL—2c LLC Mosc.* **2018**, *3*, 68–77.
68. Kalytka, V.A.; Korovkin, M.V.; Madi, P.W.; Magauin, B.K.; Kalinin, A.V.; Sidorina, E.A. Quantum-mechanical model of thermally stimulated depolarization in layered dielectrics at low temperatures. *IOP J. Phys. Conf. Ser.* **2021**, *1843*, 012011. [CrossRef]
69. Kalytka, V.; Korovkin, M.; Tatkeyeva, G.; Bashirov, A.; Bilichenko, Y.; Sidorina, Y.; Senina, Y.; Ospanov, B.; Brazhanova, D.; Baidyussenov, G.; et al. Quantum kinetic phenomena in proton semiconductors and dielectrics. In Proceedings of the 3rd International Conference on "Functional Materials and Chemical Engineering", City Seasons Suites, Dubai, United Arab Emirates, 9–10 November 2022; pp. 95–97.
70. Berry, L.G.; Mason, B. *Mineralogy: Concepts, Descriptions, Determinations*; W. H. Freeman and Company: San Francisco, CA, USA; London, UK, 1959; 612p.
71. *The Minerals Encyclopedia: 700 Minerals, Gems and Rocks*; Firefly Books: Richmond Hill, ON, Canada, 2022; 448p, ISBN-10: 0228103622, ISBN-13: 978-0228103622.
72. *The Illustrated Guide to Rocks & Minerals*, 3rd ed.; Lorenz Books: Dayton, OH, USA, 2018; 256p, ISBN-10: 0754834425, ISBN-13: 978-0754834427.
73. Dana, J.D.; Dana, E.S.; Palache, C.; Berman, H.; Frondel, C. *The System of Mineralogy*, 7th ed.; Wiley: New York, NY, USA, 1951; Volume II.